NONINVASIVE NEUROPROSTHETIC CONTROL OF GRASPING BY AMPUTEES

A Dissertation

Presented to

The Faculty of the Department of Electrical and Computer Engineering

University of Houston

In Partial Fulfillment

Of the Requirements for the Degree

Doctor of Philosophy

In Electrical Engineering

by

Harshavardhan A. Agashe

December 2014

NONINVASIVE NEUROPROSTHETIC CONTROL OF GRASPING BY AMPUTEES

Harshavardhan A. Agashe

Approved:

Chair of the Committee
Dr. Jose L. Contreras-Vidal, Professor,
Department of Electrical and Computer Engineering

Committee Members:

Dr. Haluk Ogmen, Professor,
Department of Electrical and Computer Engineering

Dr. Bhavin R. Sheth, Associate Professor,
Department of Electrical and Computer Engineering

Dr. Andrei Dragomir,
Instructional and Research Assistant Professor,
Department of Biomedical Engineering

Dr. Christian Cipriani, Assistant Professor,
Scuola Superiore Sant'Anna, Pisa, Italy

Dr. Suresh Khator, Associate Dean,
Cullen College of Engineering

Dr. Badri Roysam, Professor and Chair,
Department of Electrical and Computer Engineering

ACKNOWLEDGEMENTS

This research was supported by NSF Award # 1219321.

This dissertation is dedicated to my wife Jackie, and my parents Lalita and Ashok.

I'd like to thank all those whose direct and indirect contributions made this dissertation possible:

- My advisor Dr. Jose Contreras-Vidal (Pepe) for his guidance, mentorship and support throughout my graduate training. In addition to scientific and engineering knowledge, I have learned so much more from Pepe: staying dynamic, independent thinking, the importance of people skills, thinking and writing clearly, attention to detail, public speaking, and presentation skills.
- My dissertation committee members Dr. Haluk Ogmen, Dr. Bhavin Sheth, Dr. Andrei Dragomir, and Dr. Gerard Francisco for serving on my dissertation committee.
- Dr. Christian Cipriani for serving on my dissertation committee, and for providing the prosthetic hand for this research. He was always available for me in case of difficulties with the prosthetic hand.
- My amputee subjects for their willingness to help with my research, and their continued patience throughout the testing sessions.
- Ted Muilenburg for his help with patient recruitment and fabrication of prosthetic interfaces.
- My colleague and friend Andrew Paek for his invaluable insights and discussions.
- My peer mentor and friend Anusha Venkatakrishnan for pushing me to be on track to graduate and advising me in my job search.
- Members of the Noninvasive Brain-Machine Interface Systems Lab for their insights discussions, and support.

- My friends and roommates at Maryland whose support helped me immeasurably.
- My parents Lalita and Ashok, and my sister Deepa who have instilled in me a love for science. Their unconditional love and support have been the pillars of my personal life.
- My wife Jacqueline Agashe for carrying me through the most difficult phase of my dissertation. Her love and caring provided the support I needed to finish my thesis. Even after long and stressful days, she would be understanding and patient, and always cheered me up. I am grateful to her for always being there for me.

NONINVASIVE NEUROPROSTHETIC CONTROL OF GRASPING BY AMPUTEES

An Abstract

of a

Dissertation

Presented to

The Faculty of the Department of Electrical and Computer Engineering

University of Houston

In Partial Fulfillment

Of the Requirements for the Degree

Doctor of Philosophy

In Electrical Engineering

by

Harshavardhan A. Agashe

December 2014

ABSTRACT

Smooth coordination and fine temporal control of muscles by the brain allows us to effortlessly pre-shape our hand to grasp different objects. Correlates of motor control for grasping have been found across wide-spread cortical areas, with diverse signal features. These signals have been harnessed by implanting intracortical electrodes and used to control the motion of robotic hands by tetraplegics, using algorithms called brain-machine interfaces (BMIs). Signatures of motor control signal encoding mechanisms of the brain in macro-scale signals such as electroencephalography (EEG) are unknown, and could potentially be used to develop noninvasive brain-machine interfaces. Here we show that a) low frequency (0.1 – 1 Hz) time domain EEG contains information about grasp pre-shaping in able-bodies individuals, and b) This information can be used to control pre-shaping motion of a robotic hand by amputees. In the first study, we recorded simultaneous EEG and hand kinematics as 5 able-bodies individuals grasped various objects. Linear decoders using low delta band EEG amplitudes accurately predicted hand pre-shaping kinematics during grasping. Correlation coefficient between predicted and actual kinematics was r = 0.59 ± 0.04, 0.47 ± 0.06 and 0.32 ± 0.05 for the first 3 synergies. In the second study, two transradial amputees (A1 and A2) controlled a prosthetic hand to grasp two objects using a closed-loop BMI with low delta band EEG. This study was conducted longitudinally in 12 sessions spread over 38 days. A1 achieved a 63% success rate, with 11 sessions significantly above chance. A2 achieved a 32% success rate, with 2 sessions significantly above chance. Previous methods of EEG-based BMIs used frequency domain features, and were thought to have a low signal-to-noise ratio making them unsuitable for control of dexterous tasks like grasping. Our results demonstrate that time-domain EEG contains information about grasp pre-shaping, which can be harnessed for neuroprosthetic control.

TABLE OF CONTENTS

LIST OF FIGURES

Chapter 2

Chapter 3

CHAPTER 1: INTRODUCTION

Limb loss due to amputation results in a severe reduction in the quality of life of affected individuals. In upper limb amputees, grasping is one of the most important yet challenging functions a prosthetic hand is required to perform. Advances in robotics have made it possible to achieve dexterous control in an anthropomorphic robotic hand (Cipriani et al., 2011a, 2011b). Body-powered prosthetic control strategies are reliable and have essentially remained unchanged for the past 100 years, while recent advances in myoelectric control (Kuiken et al., 2009; Cipriani et al., 2011a) offer promise with improved ease of use.

Brain machine interfaces (BMIs) which directly translate neural activity to control external devices can add intuitive and natural control to myoelectric devices (Contreras-Vidal et al., 2012). Intracortical BMIs, in which cortical signals are obtained through implanted microelectrode arrays, have been demonstrated to control arm positioning with a high degree of accuracy in monkeys and tetraplegic humans, but have a single degree of freedom to control grasping (Hochberg et al., 2012; Collinger et al., 2012; Velliste et al., 2008). Implementing an intuitive and noninvasive BMI for grasping has remained a challenge, however.

To successfully implement noninvasive BMIs for grasping prosthetic devices in amputees, the first step is to understand where and how motor commands associated with grasping are encoded in macro-scale cortical activity. Correlates of motor control for grasping have been found across wide-spread cortical areas, with diverse signal features. These signals have been harnessed by implanting intracortical electrodes and used to control the motion of robotic hands by tetraplegics, using BMI algorithms. Signatures of motor control signal encoding mechanisms of the brain in macro-scale signals such as electroencephalography (EEG) are unknown, and could potentially be

used to develop noninvasive brain-machine interfaces for use by amputees or other clinical populations with impaired hand function.

Proximal and distal upper extremity movement information has been shown to be encoded as the power in specific frequency bands in cortical field potentials at different spatial scales: local field potentials (LFPs), electrocorticography (ECoG), electroencephalography (EEG) and magnetoencephalography (MEG) (Zhuang et al., 2010; Kubánek et al., 2009; Pistohl et al., 2012; Ball et al., 2008; Waldert et al., 2009). More recently, researchers have shown that information is also encoded in the time-domain amplitudes of these field potentials in the lowest frequency band (0-5 Hz) (Mollazadeh et al., 2011; Bansal et al., 2011; Acharya et al., 2010; Kubánek et al., 2009; Bradberry et al., 2010, 2009; Hall et al., 2014). In Chapter 2, we show that grasping movements in able-bodied individuals can be decoded from time-domain low delta-band (0.1 – 1 Hz) electroencephalographic (EEG) activity, a noninvasive modality to record cortical potentials at the scalp (Agashe and Contreras-Vidal, 2011, 2013a). Further, we showed that principal components (PCs) of finger kinematics are decoded with the same level of accuracy as finger joint angles during grasp pre-shaping. In a closed-loop BMI scenario, it is advantageous to control the kinematic PCs as they allow grasp pre-shaping with fewer degrees of freedom.

Chapter 3 is an application of the encoding mechanisms shown in Chapter 2 to control a closed-loop prosthetic device in real time. Signal to noise ratio and reliability across sessions in EEG have been concerns which may be inapplicable in the case of low frequency time-domain EEG. In chapter 3 we demonstrate dexterous neuroprosthetic control of grasping with EEG signals by amputees and address these concerns by investigating stability of EEG signals as well as changes in BMI performance over multiple sessions performed on different days.

CHAPTER 2: GLOBAL CORTICAL ACTIVITY PREDICTS SHAPE OF HAND DURING GRASPING

2.1 Introduction

Grasping is one of the most fundamental ways humans interact with the world, allowing us to manipulate and interact with objects around us. The kinematics of grasping and the neuroscience underlying the smooth and continuous control of the hand and fingers have been studied extensively (Jeannerod, 1984; Castiello, 2005; Santello et al., 2002), and experiments have shown modulation in neural spiking activity associated with various stages of grasping (Bansal et al., 2011; Rizzolatti et al., 1988; Murata et al., 1997). PET and fMRI experiments show the involvement of widely distributed brain areas during a self-initiated grasping movement (Castiello, 2005). Proximal and distal upper extremity movement information has been shown to be encoded as the power in various frequency bands in cortical field potentials at various spatial scales, such as local field potentials (LFPs), electrocorticography (ECoG), electroencephalography (EEG) and magnetoencephalography (MEG) (Zhuang et al., 2010; Kubánek et al., 2009; Pistohl et al., 2012; Ball et al., 2008; Waldert et al., 2009). More recently, researchers have shown that information is also encoded in the time-domain amplitudes of these fields in the lowest frequency band (0-5 Hz) (Mollazadeh et al., 2011; Bansal et al., 2011; Acharya et al., 2010; Kubánek et al., 2009; Bradberry et al., 2010, 2009; Hall et al., 2014). It remains unclear if these amplitude modulations contain enough information to be able to infer the dexterous movement of the fingers during grasping, at the macro scale of scalp EEG.

LFP modulations have been shown to contain information about grasping movements not just in the primary motor cortex, but in a multitude of other brain areas as well (Bansal et al., 2011; Mollazadeh et al., 2011; Hall et al., 2014). While it is clear that a widely distributed network involving pre-frontal, sensori-motor as well as visuo-

motor areas in both hemispheres is responsible for the control of self-initiated grasping actions (Matsumura et al., 1996; Rizzolatti et al., 1996), the characterization of scalp-level neural representations of these areas remains unknown. Recent findings revealed cyclic activity in motor cortex LFP signals locked to 'submovements' (Hall et al., 2014). Understanding how these delta band (0-4 Hz) submovements combine to yield functional motion may provide clues to the origins of delta-band activity and why they encode upper limb movement information (Hall et al., 2014).

Apart from the neuroscience community, being able to decode grasping kinematics is of great interest to the brain-machine interface (BMI) community. Upper limb amputation, stroke, or severe spinal cord injury result in loss or significant reduction in bimanual motor function and dexterous hand movements in the affected limb(s). Improved upper extremity function is the leading requirement among tetraplegics (Snoek et al., 2004) and other clinical populations with impaired hand function. Control of hand prosthetics with peripheral signals such as intramuscular/surface electromyography (sEMG) (Cipriani et al., 2011a, 2014) and targeted muscle re-innervation (Kuiken et al., 2009) show promise. Brain-machine interfaces which extract movement intent from brain activity and control external devices are another possible strategy to regain hand function (Lebedev and Nicolelis, 2006; Birbaumer, 2006) while also tracking plasticity in the brain. Current upper limb neuroprosthetics restore some degree of functional ability, but fail to approach the ease of use and dexterity of the natural hand, particularly for grasping movements. Control of an anthropomorphic robotic arm with intracortically recorded neural activity was recently shown to be possible (Hochberg et al., 2012; Collinger et al., 2012). These invasive BMI systems are able to extract intended arm position and movement in space, along with a control over opening and closing a grasp. However, the multitude of grasp types required in activities of daily living require a detailed level of control over manual dexterity and grasp posture. Further, the inherent

risks associated with surgery required to implant electrodes, along with the long-term stability of recorded signals, is of concern (Schultz and Kuiken, 2011). Current approaches to noninvasive BMIs typically require the user to learn to control the power in their sensorimotor mu-rhythms (specific frequency bands usually centered around 10 Hz and 22 Hz) (Wolpaw and McFarland, 2004; McFarland et al., 2010). Here we show that it is feasible to extract detailed information on intended grasping movements to various objects in a natural, intuitive manner, from a plurality of scalp EEG signals.

Research shows that to manipulate the large number of joints available in the hand during grasping, the motor system controls an inherently low-dimensional manifold called the synergy space (Santello et al., 2002, 1998; Vinjamuri et al., 2010). A common approach to identifying these movement synergies is by decomposing joint angle velocities into their Principal Components (PCs) (Santello et al., 1998). The kinematic space (joint angle velocities vs. movement synergies) that is optimally encoded in cortical field potentials remains unknown. In this study, five human subjects performed self-initiated and natural reach-to-grasp movements to five common objects while EEG and hand kinematics were recorded simultaneously. We selected five objects requiring distinct types of grasps: a soda can (cylindrical power grasp), a CD (whole hand circular grasp), a credit card (lateral precision grasp), a small coin (precision pinch grasp) and a screwdriver (tool power grasp) (Santello et al., 1998). In an offline analysis, we reconstructed the trajectories of the hand in both joint angle velocity and synergy (PC) spaces during the grasping movement. The decoding was performed with a linear regression model with lags (i.e., time delay between EEG and decoded kinematics; see Methods). Notably, the time-domain feature space, coupled with the linear decoder, requires that the EEG signals share the same frequency bandwidth as the movement kinematics. The majority of power in grasping movements performed by subjects in this

study was concentrated in the 0.1-1 Hz band (see Methods), requiring that EEG be low-pass filtered at 1 Hz as well (see Methods).

2.2 Methods

Data acquisition and experiment design

The Institutional Review Board (IRB) at the University of Houston approved this research. Five healthy right-handed volunteers (4 males, 1 female; ages 20-28 years) participated in this study after giving written informed consent. Whole head 64-channel EEG with a 10-20 system layout (Brain Vision LLC, USA) and hand kinematics were recorded simultaneously at 1000 Hz using BCI2000 software (Schalk et al., 2004), while participants performed an object grasping task. The trajectories of 18 hand joint angles were recorded with a data glove (CyberGlove Systems LLC, USA). The following 15 joint angles were recorded and used for further processing: metacarpo-phalangeal (MCP) and proximal inter-phalangeal (PIP) joints for the four fingers; carpo-metacarpal (CMC), metacarpo-phalangeal (MCP) and interphalangeal (IP) joint for the thumb; and abduction/adduction (ABD) between the fingers. In addition, 3 more joints were recorded but not used for further processing: flexion/extension and abduction/adduction of the wrist; and palm arch which measures the curvature across the palm. An accelerometer mounted on the wrist was used to record hand transport in three subjects (subjects S1, S2 and S3).

During the behavioral task, subjects were seated behind a table with their hand resting on a push-button, which was used to detect movement onset and offset. In front of the push-button, objects were presented on a visually marked area on the table's surface. The distance between the object and the push-button were determined such that subjects were able to reach the objects comfortably. One of five objects (soda can, credit card, CD, US penny, and a screwdriver) was placed on the marked area in a pseudorandom sequence. Subjects were instructed to start each trial with a relaxed

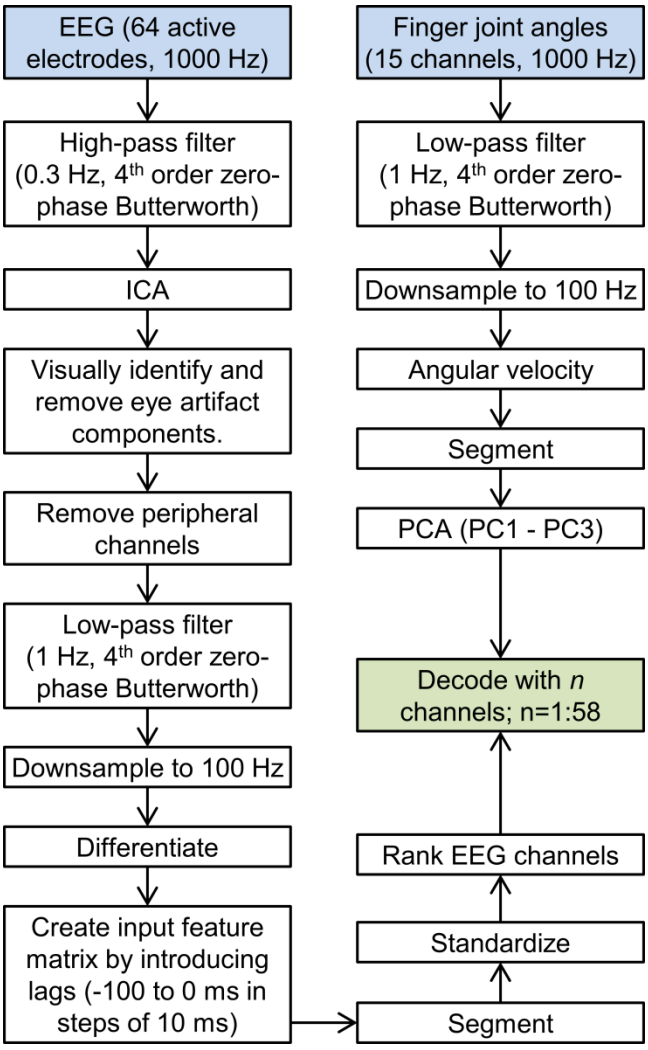

Figure 2.1 Data processing flowchart. The flowchart showing all data processing steps leading up to the decoding is shown. The left stream corresponds to EEG processing, and the right stream corresponds to kinematics processing.

gesture on the switch, then self-initiate a reach and grasp movement to the object, followed by release and back to the resting position, at their preferred speed. The mean movement time was 1.9 ± 0.3 s across all subjects. Each subject performed 250 trials (50 trials per object), except subject S4 who performed 270 trials.

EEG data preprocessing

All following analyses were performed in MATLAB (The MathWorks Inc., USA). Raw EEG data were detrended and high-pass filtered at 0.3 Hz with a zero-phase 4th

order Butterworth filter to remove amplifier drift and ultra-low frequency components (Figure 2.1). Independent component analysis (ICA) was used to decompose the EEG into statistically independent components using the EEGLAB toolbox (Delorme and Makeig, 2004) after manually removing data segments corrupted by movement artifacts. Independent components corresponding to eye blinks and eye movements were identified and removed, followed by a projection back to the scalp EEG space. Six peripheral channels (M1, M2, TP9, TP10, PO9 and PO10) were excluded from further analysis. EEG data were low-pass filtered at 1 Hz with a zero-phase 4^{th} order Butterworth filter. These filter cutoffs (0.3 – 1 Hz) were chosen based on previous findings (Agashe and Contreras-Vidal, 2011; Bradberry et al., 2010; Garipelli et al., 2013). EEG data were downsampled to 100 Hz (for faster computations) and differentiated. Temporally lagged versions of EEG were concatenated along the third dimension, for a total of 11 lags (10 to 0 samples, corresponding to 100 to 0 ms in steps of 10 ms), resulting in an $n \times 58 \times 11$ data matrix, with the first dimension corresponding to time, the second dimension to EEG channels and the third dimension to lags. Continuous EEG was segmented into trials, from 400 ms before movement onset to 100 ms after movement offset and standardized by subtracting the mean and dividing by standard deviation across all trials.

Kinematics data preprocessing

Fifteen hand joint angles were recorded at 1000 Hz synchronously with EEG data. The joint angle data were lowpass filtered at 1 Hz with a 4^{th} order zero-phase Butterworth filter, followed by downsampling to 100 Hz (Figure 2.1). The change introduced due to filtering the kinematics was quantified using the signal-to-error ratio (SER) defined as $SER(y, y^*) = 10\log_{10}\frac{Var(y)}{MSE(y,y^*)}$, where y is the raw kinematics, y^* is the filtered kinematics, Var denotes the variance and MSE is the mean square error. The

mean SER across all blocks was found to be 15.5 ± 2.9 dB ensuring filter cutoffs were appropriate. Joint angles were then differentiated to yield angular velocities. Kinematics were segmented consistent with EEG (400 ms before movement onset to 100 ms after movement offset). Principal Component Analysis (PCA) was used to decompose the joint angular velocities into kinematic synergies, across all trials. The input to the PCA matrix consisted of an $n \times 15$ matrix, where n is the sum of trial lengths. The first three synergies accounted for 90 ± 1 % of the variance and were retained for decoding. Individually, the first three synergies accounted for 50 ± 1 %, 29 ± 1 % and 10 ± 1 % of the variance.

Decoding

A Wiener filter was used to continuously decode joint angle velocity PCs:

$$PC_i[t] = \beta_{0i} + \sum_{n=1}^{N}\sum_{k=0}^{L}\beta_{nki}EEG_n[t-k],$$

where $PC_i[t]$ is the i^{th} PC ($i = 1,2,3$ for the first three PCs), β_{nki} are the model parameters, $N = 1\ to\ 58$ are the number of EEG channels used for decoding, L is the maximum time lag (100 ms) and $EEG_n[t-k]$ is the preprocessed EEG value of the n^{th} channel at time $t-k$.

Within each subject, an 8-fold cross validation procedure was employed to assess the decoding accuracy: data were divided into eight parts, with the i^{th} part designated as testing data in the i^{th} cross validation fold (a total of eight folds). The remaining seven parts in a cross validation fold constituted the training data for that fold. For each cross-validation fold, model parameters were calculated on training data by minimizing the square error between the observed and model-estimated values for each PC. These model parameters were then applied to pre-processed EEG from the testing set to obtain a prediction of the PC value. We report the median correlation coefficient

between the predicted and the observed PC values across all folds as the metric to assess decoding accuracy.

We evaluated the dependency of the decoding accuracy on the number of EEG channels used for the decoding process by the following procedure. Preprocessed EEG channels were ranked according to how well they were correlated with the three kinematic principal components (PCs), averaged over all lags. Specifically, the metric used for ranking was

$$R_n = \frac{1}{L+1}\sum_{k=0}^{L}\sqrt{\beta_{nkPC1}^2 + \beta_{nkPC2}^2 + \beta_{nkPC3}^2}\,,$$

where R_n is the metric for the n^{th} EEG channel and β are the regression parameters calculated over the entire dataset for each subject (Bradberry et al., 2010). The 8-fold cross validation decoding procedure was then performed iteratively using the best N EEG channels ($N = 1\ to\ 58$) according to the channel ranking metric described above.

We assessed the contribution $\%T_i$ at each lag i ($i = 0\ to 100\ ms$) as

$$\%T_i = 100\% \times \frac{\sum_{n=1}^{N}\sqrt{\beta_{nkPC1}^2+\beta_{nkPC2}^2+\beta_{nkPC3}^2}}{\sum_{k=0}^{L}\sum_{n=1}^{N}\sqrt{\beta_{nkPC1}^2+\beta_{nkPC2}^2+\beta_{nkPC3}^2}}.$$

We plotted the contributions from EEG channels at each lag on a scalp map to graphically assess the evolution of sensor contributions with time.

Discrete classification

To quantify the information content of EEG to discriminate between the grasp types, we constructed a multiple kernel learning (MKL) classifier (Gönen and Alpaydın, 2011; Rakotomamonjy et al., 2008), which is a multiple-kernel generalization of support vector machines (SVM). The key idea of MKL is to replace the single kernel in a SVM by a weighted linear combination of different basis kernels. The scalp was divided into 8 regions of interest (ROIs): left frontal (LF), right frontal (RF), left temporal (LT), right temporal (RT), left sensori-motor (LSM), right sensori-motor (RSM), left parietal-occipital

(LPO), and right parietal-occipital (RPO). The combined kernel function $K(x_i, x_j)$ for input feature samples x_i and x_j was represented as

$$K(x_i, x_j) = \sum_{m=1}^{M} d_m K_m(x_i, x_j),$$

such that $d_m \geq 0$, and $\sum_{m=1}^{M} d_m = 1$, where $M = 24$ is the number of basis kernels and d_m is the weight for the m^{th} basis kernel K_m. Parameters d_m were optimized through gradient descent on an SVM-based objective function according to "SimpleMKL" algorithm (Rakotomamonjy et al., 2008). Radial basis functions with relative width parameter $\sigma = \{5, 10, 15\}$ were used as basis kernels for each of the 8 ROIs, resulting in a total of 24 basis kernels. This range of values was found to be reasonable after applying kernel alignment to an initial training set for each subject (Shawe-Taylor and Kandola, 2002). The input features for the discrete classifier were identical to the Wiener filter decoder detailed above, i.e., low frequency time-domain EEG, lagged from 0 to 100 ms.

The information content in EEG was calculated as the reduction in entropy of the probability distribution over grasp types (Quian Quiroga and Panzeri, 2009):

$$I = \sum_{PG,MG} P(PG, MG) \log_2 \frac{P(PG, MG)}{P(PG)P(MG)},$$

where I is the information content in EEG about the grasp type; $P(PG, MG)$ is the joint probability over predicted grasp type PG and measured grasp type MG, calculated from the confusion matrix of the classifier; $P(PG)$ and $P(MG)$ are the marginal probabilities. We calculated the information content from -1 to 3 seconds with respect to movement onset, in steps of 250 ms (Figure 2.6). For each time step, an 8-fold cross validation scheme was used, and the results shown (Figure 2.6) are the median values of information over testing folds. The classifier confusion matrix at 250 ms is shown in Figure 2.6.

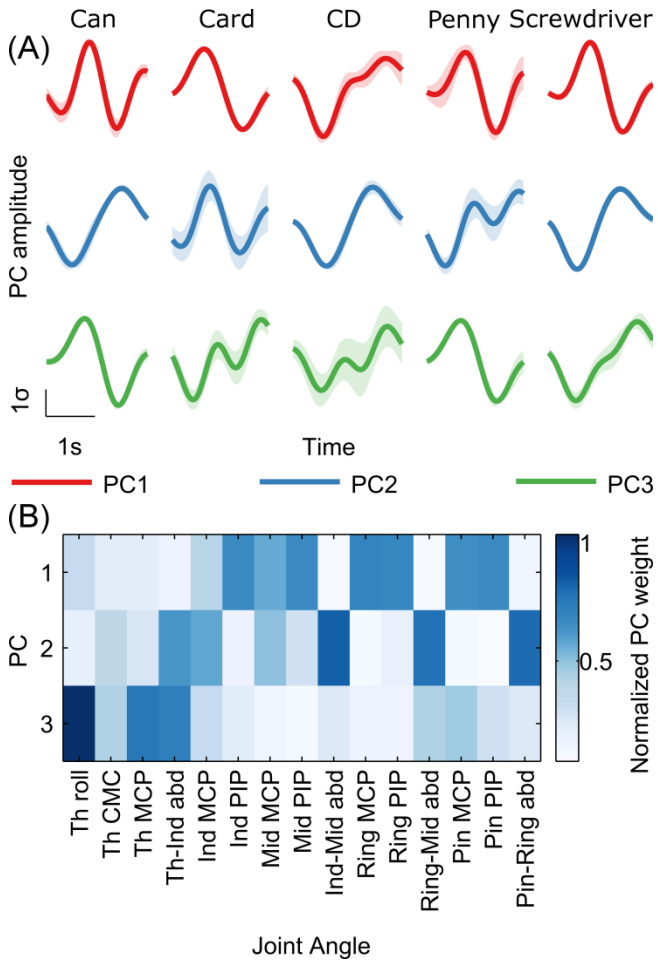

Figure 2.2 Kinematic trajectories show synergies while grasping objects. (A) Mean principal component (PC) amplitudes (± s.e.m; shaded regions) are shown for the first three PCs in subject S5. (B) PC loading on the fifteen joint angles are shown for the first three

2.3 Results

Both joint and synergy spaces can be decoded from scalp EEG

Previous studies point to both joint angular velocities as well as synergies as possible spaces in which the brain encodes grasping movement information (Acharya et al., 2010; Kubánek et al., 2009; Vargas-Irwin et al., 2010; Agashe and Contreras-Vidal, 2011; Pistohl et al., 2012). Here, we found high decoding accuracies for both joint angle velocities and their synergies. Movement synergies were calculates as the principal components (PCs) of joint angular velocities across all grasp types (Santello et al., 1998;

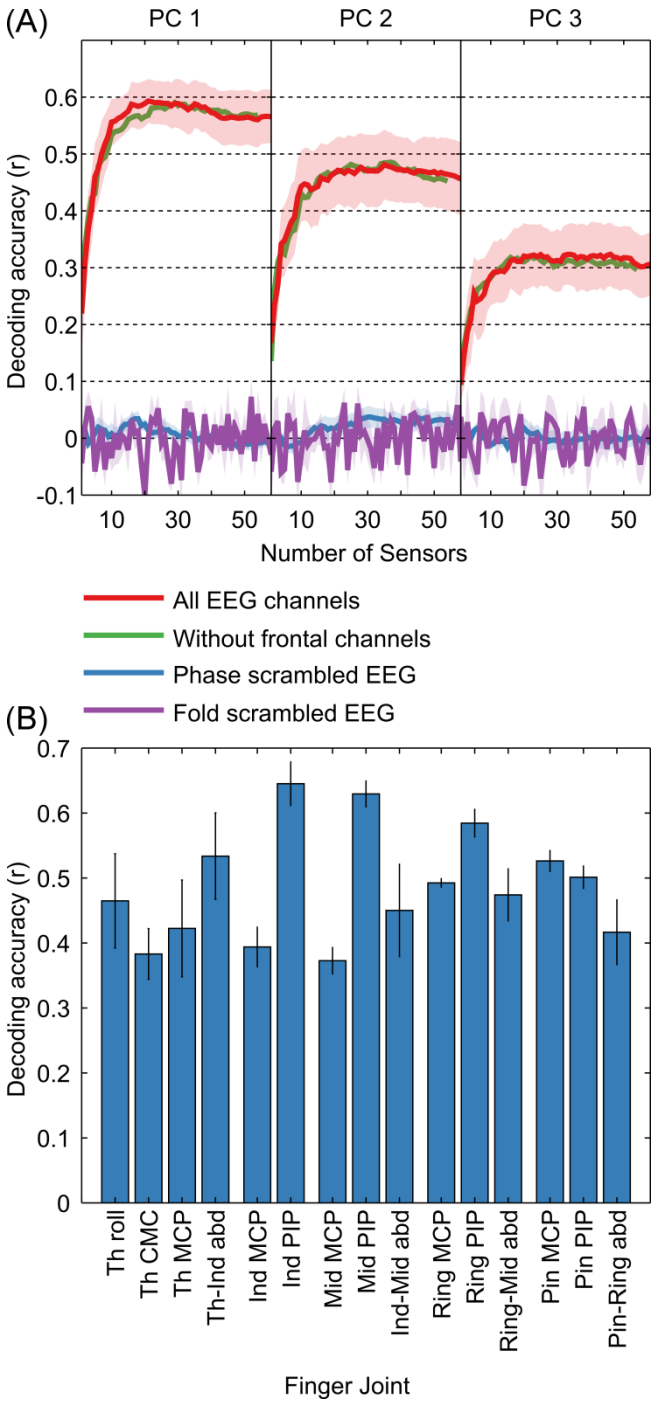

Figure 2.3 Decoding Accuracies. (A) Mean decoding accuracies across subjects are shown in red (± s.e.m; shaded regions) for PC1, PC2 and PC3. (B) Mean decoding accuracies for all joint angles (± s.e.m; errorbars).

Vinjamuri et al., 2010). We retained the first three PCs, which retained 90% of the variance. Figure 2.2 shows examples of PC trajectories across all objects and the

visualization of PC loadings on each joint angle. PC1 was highly loaded on the finger PIP and MCP joints representing grasp opening/closing motion. PC2 was loaded mainly on the abduction joints, representing the spreading motion of the hand. PC3 was loaded on the thumb joints, mainly rotation, and represents the independent movement of the thumb.

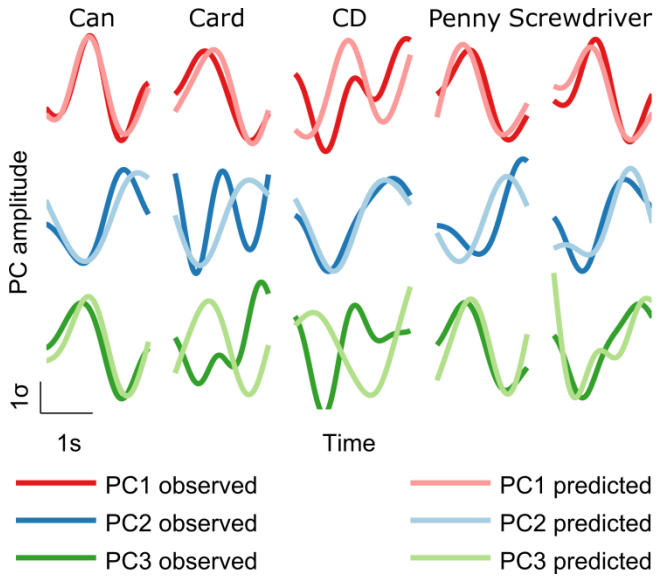

Figure 2.4 Decoded trajectories. Predicted trajectories (light traces) showed similarity with measured trajectories (heavy traces). Examples of decoded PC trajectories for each object are shown for subject S5.

Decoding accuracies were quantified as the median correlation coefficient between the predicted and measured kinematics across cross validation folds. For each subject, we calculated decoding accuracies across the best $\boldsymbol{n}$ channels, with $\boldsymbol{n}$ ranging from 1 to 58, to evaluate the dependence of decoding accuracy on the number of EEG channels used. The common pattern across all decoded kinematics was a rapid initial increase followed by saturation/slow decrease (Figure 2.3). To determine the peak in a robust manner, we fit a double exponential to the curves. For PC1, PC2 and PC3, peak decoding accuracies (mean ± s.e.m) were r = 0.59 ± 0.04, 0.47 ± 0.06 and 0.32 ± 0.05, with the peaks occurring when 22, 29 and 27 EEG channels were used to decode,

respectively. Examples of decoded PC trajectories are shown in Figure 2.4. For individual joint angle velocities, we found that peak decoding accuracies were highest for the index, middle and ring PIP joints (r = 0.65 ± 0.03, 0.63 ± 0.02 and 0.58 ± 0.02) and lowest for thumb CMC, index MCP and middle MCP joints (r = 0.38 ± 0.04, 0.39 ± 0.03 and 0.37 ± 0.02). The mean decoding accuracy across all joints was r = 0.49 ± 0.02. The decoding accuracies for joint angles and kinematic PCs are comparable, indicating that both kinematic spaces may be equally encoded in EEG-based sensor space. These decoding accuracies are comparable to results from ECoG studies (r = 0.52 for first synergy; Acharya et al., 2010) and intracortical studies in monkeys (r = 0.62 for grasp aperture and r = 0.46 for aperture velocity; Zhuang et al., 2010).

Decoding accuracies were highly significant ($p<0.001$; Bonferroni corrected for multiple comparisons across all subjects, kinematic variables, number of EEG channels and cross validation folds). We also calculated empirical chance levels using two methods: 1) by scrambling the phase of the EEG (Theiler et al., 1992) and 2) by scrambling the EEG trial indices (Antelis et al., 2013). 'Phase-scrambled' EEG signals were obtained by randomizing the phase in the Fourier domain, while keeping the magnitude unchanged, followed by a transformation back to the time domain. The assumption behind time-domain decoding is that EEG signals are phase-locked to the kinematics, and a randomization of the phase would theoretically result in zero decoding accuracy. In the case of 'fold-scrambled' EEG, the pairing between EEG and kinematics across trials was randomized, so that EEG corresponding to the kinematics from trial $\boldsymbol{n}$ was assigned to trial $\boldsymbol{m}$. The expected decoding accuracy in this case is also close to zero. The decoding procedure as detailed in the methods section was applied to the 'phase-scrambled' and 'fold-scrambled' EEG signals, and we found close to zero decoding accuracy in both cases (Figure 2.3), showing that the decoding accuracy obtained without scrambling is significantly higher than chance levels.

Artifacts did not aid decoding

EEG is known to be affected by ocular and muscular artifacts (Goncharova et al., 2003), which may contribute to decoding if they are task-correlated. In our experiment, muscular artifacts are unlikely to affect decoding results because we low-pass filtered EEG signal at 1 Hz, and the frequency content of muscular artifacts is above 8 Hz (Goncharova et al., 2003). We prevented ocular artifacts from affecting our results in two stages: 1) by using Independent Component Analysis (ICA) to identify and remove ocular artifacts (Delorme and Makeig, 2004), as detailed in the methods section, and 2) by experiment design: All objects to be grasped were presented to subjects in the same spatial location, likely resulting in identical eye movements for all objects, making it unlikely that such a common pattern across objects could distinguish between them. To show the efficacy of these steps, we ran the decoding procedure without the four frontal channels affected most by ocular artifacts (FP1, FP2, AF7 and AF8). The decoding accuracy was unchanged (Figure 2.3), demonstrating that ocular artifacts did not affect our decoding results.

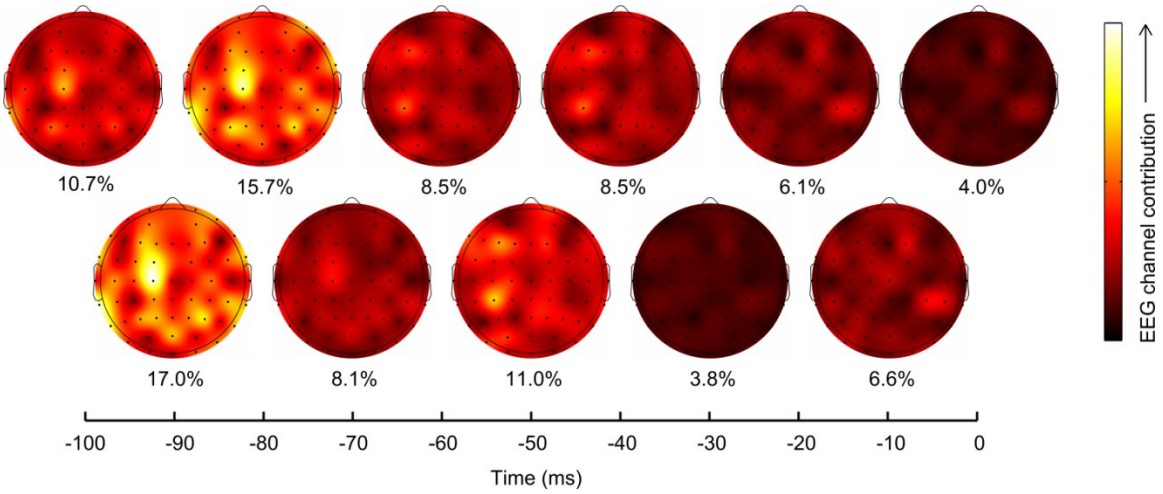

Figure 2.5 Scalp locations and lags contribution to PC1 prediction. The overall percentage contribution of each lag is shown below each scalp map. Lags -90 and -80 ms contributed maximally, particularly with EEG channels C1, FC1, P1 and P3.

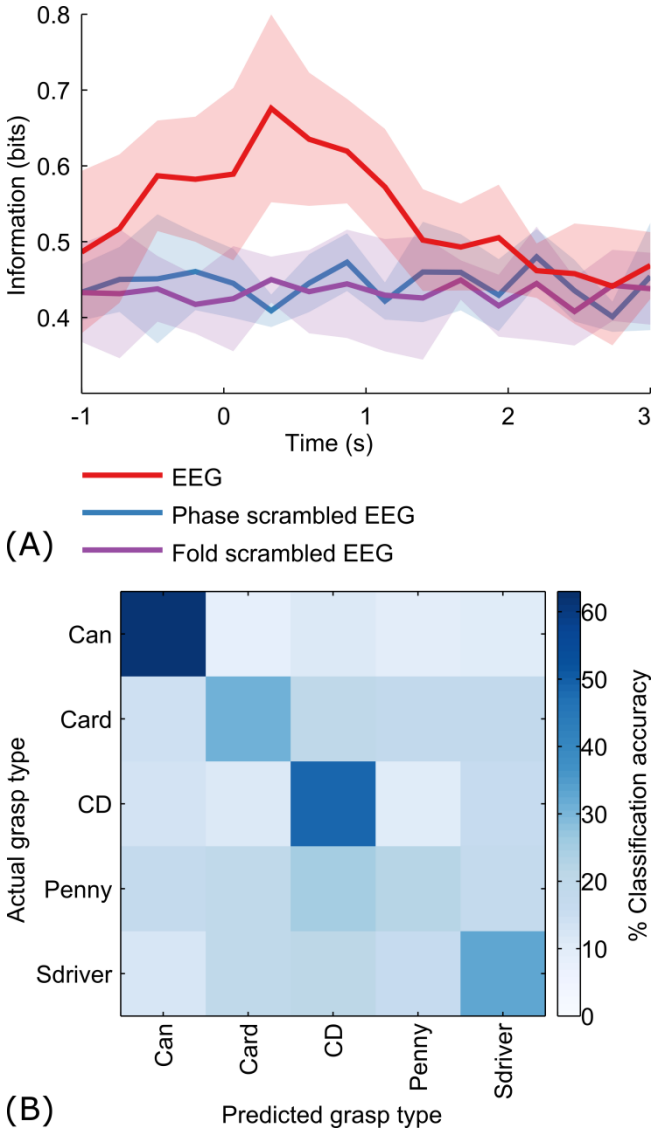

Figure 2.6 Information content in EEG. (A) Information in EEG peaked at around 250 ms after movement onset. (B) The classifier confusion matrix at 250 ms after movement onset is diagonal, indicating high classification accuracies.

Neural representation of grasping kinematics in sensor space

To assess which scalp regions contributed the most to kinematics prediction, we plotted the contribution of EEG channels (see Methods section) at each time lag on a scalp map, for PC1 (Figure 2.5), as PC1 accounted for 50 ± 1 % of the joint velocity variance and was also the best decoded synergy. Lags -90 and -80 ms contributed maximally (17.0% and 15.7%), particularly at scalp locations C1, FC1, P1 and P3.

Interestingly, C1 and FC1 are located above the primary motor cortex and supplementary motor areas, which may explain their high contributions. P1 and P3 lie above the associative cortices which process the visuo-motor transformations necessary for a reach-and grasp movement. In agreement with established neuroscience findings, the contralateral hemisphere made the highest contribution. However, motor areas from the ipsilateral hemisphere (C5, P5 and CP7) also made contributions. At around -60 to -40 ms, CP5 played the major role in decoding PC1 kinematics. Transient recruitment of specific EEG channels primarily between -90 to -40 ms argues against movement artifacts inadvertently aiding the decoding process, since movement artifacts are expected to correlate maximally with movement at zero lag.

Grasp classification peaked 250 ms after movement onset

The decoding accuracies shown represent the prediction of the finger joint velocities/PCs, and can be implemented directly to control the grasping motion of a prosthetic hand. A hybrid approach could conceivably be used as well, in which the grasp type is predicted as a discrete class from EEG, based on which a pre-determined grasp trajectory can be implemented. A metric that measures the performance of such a classification-based motor prosthesis is the information (in bits) conveyed about the grasp type. We constructed multiple kernel learning classifiers (see Methods) to classify 100 ms windows of EEG into discrete grasp types. When applied over the grasp duration, from -1 to 3 seconds with respect to movement onset, the information content in EEG peaked at 250 ms (Figure 2.6). This is in agreement with a previous study (Pistohl et al., 2012) which showed similar results with ECoG (electrocorticographic) data over a two-class grasp (precision vs. power) problem. For our five-class problem, the maximum information was 0.68 bits, occurring 250 ms after movement onset. The mean confusion matrix across subjects at 250 ms is shown in Figure 2.6. The classifier confusion matrix at 250 ms after movement onset is diagonal, indicating high

classification accuracies. Precision grasps were decoded at a lower classification accuracy (27%; card, penny) than whole-hand grasps (48%; can, CD, screwdriver). Surprisingly, a penny (precision grasp) was often misclassified as a CD (whole hand circular grasp), possibly due to the similarity in their kinematic trajectory shapes (Figure 2.2A), despite the differences in amplitude. The overall decoding accuracy was 40% across the 5 objects, with chance level at 20%.

2.4 Discussion

Delta-band time domain EEG encodes grasping kinematics

Recent studies on monkeys and humans attempted to decode various aspects of grasping such as joint angles or grasp types from brain activity recorded through microelectrode arrays implanted in the brain or electrocorticographic (ECoG) grids placed over the cortex (Acharya et al., 2010; Kubánek et al., 2009; Pistohl et al., 2012; Vargas-Irwin et al., 2010; Agashe and Contreras-Vidal, 2011; Artemiadis et al., 2007; Hamed et al., 2007; Zhuang et al., 2010; Saleh et al., 2010; Townsend et al., 2011; Aggarwal et al., 2008). Activity of multiple neurons in the motor cortex has been shown to classify finger and wrist movements as well as grasp patterns (Artemiadis et al., 2007; Hamed et al., 2007; Aggarwal et al., 2008). Interestingly, individuated finger movements and movements during slow grasping motion can be predicted from the fluctuations of low-pass filtered (the so-called “local motor potential” or LMP) ECoG activity in humans (Acharya et al., 2010; Kubánek et al., 2009). Accurate classification of precision vs. whole-hand grip has also been shown with ECoG LMP (Pistohl et al., 2012). A recent study showed that motor networks controlling the upper limb exhibit an intrinsic periodicity at submovement frequencies in the delta band (0.1 – 4 Hz) that is reflected in the speed profile of movements (Hall et al., 2014). The present results, obtained using low-frequency time domain features, suggest that such an encoding mechanism, based

on amplitude modulation, is observed in non-invasively recorded macro-scale level brain activity as well (Figure 2.3).

Relevance to clinical populations and brain-machine interfaces

The spatial locations of highly contributing electrodes over multiple lags over the scalp suggest early recruitment of the contralateral frontal-central scalp areas and parietal electrodes, followed by involvement of the central electrodes over primary sensorimotor cortical areas (Figure 2.5). This pattern of spatiotemporal information processing is in agreement with previous studies (Castiello, 2005). Changes in these spatial patterns of neural activity, at the level of scalp electrodes, may provide a window to investigate the plasticity of the brain during learning to use a brain-machine interface (BMI). These maps of predictive electrodes may also be informative when compared to those from clinical populations. The high values and significance levels of the decoding accuracies (Figure 2.3) argue against the need for more localized means of extracting neural activity for decoding, and suggest that information about dexterous grasping movements are represented in fast-changing global networks at the EEG scale. Importantly, these findings merit further investigation to assess the feasibility of EEG-based decoding for closed-loop BMI systems to control dexterous neuroprosthetics.

The high decoding accuracies obtained in this study suggest that this methodology is a promising candidate for application in real-time closed loop BMI systems for inferring desired grasping movements. We obtained similar levels of decoding for individual joint angles and synergies based on PCs, which suggests that a PC-based control scheme requiring lesser degrees of freedom is advantageous over individual joint angle control for closed-loop control of a hand neuroprosthesis. We are cognizant that effective BMI systems require decoding of movement intent in the absence of real movement. In this regard, recent studies demonstrated reach and grasp by tetraplegics using a neurally (intracranial electrodes) controlled robotic arm, albeit not

as fast or accurate as those of an able-bodied person (Hochberg et al., 2012; Collinger et al., 2012). Although the present study deciphers the cortical EEG signatures of actual movement, it is likely that some neural characteristics or features may be shared between imagined and real movements (Hochberg et al., 2012; Yuan et al., 2010; Bradberry et al., 2011; Agashe and Contreras-Vidal, 2013b). Results from a few studies suggest that with training, patients could regain control of neural populations that would otherwise participate in natural movements for the purpose of a BMI (Hochberg et al., 2012; Collinger et al., 2012; Hochberg et al., 2006). Our methodology could also help to elucidate the changes in the neural representation for movement during skill learning or during intervention to rehabilitate fine motor control after brain injury. Importantly, our results challenge the perceived limitations of scalp EEG as a source signal for BMI systems or their use to investigate cortical plasticity during imagined or performed motor acts.

In this study we decode with a simple linear model as they have been shown to provide high decoding accuracies from a multitude of brain signals (spiking activity, LFP, ECoG, EEG and MEG) (Mollazadeh et al., 2011; Acharya et al., 2010; Bradberry et al., 2010, 2008). Dexterous tasks like handwriting have been reconstructed from electromyographic (EMG) signals from the hand with linear filters (Linderman et al., 2009). While evidence is mounting for the time-domain encoding mechanism in field potentials, more research is needed to elucidate its relationship with frequency domain representations and spiking activity (Bansal et al., 2011). Further research is also required to characterize the consistency of the channel selections made across subjects, and to investigate the role of higher frequencies for EEG decoding.

CHAPTER 3: NONINVASIVE NEUROPROSTHETIC CONTROL OF GRASPING BY UPPER LIMB AMPUTEES

3.1 Introduction

Upper limb amputation, stroke, or severe spinal cord injury result in loss or significant reduction in bimanual motor function and dexterous hand movements in the affected limb(s). Improved upper extremity function is the leading requirement among tetraplegics (Snoek et al., 2004) and other clinical populations with impaired hand function. Recent advances in robotic prosthetics for the upper limb potentially allow amputees to control a multitude of dexterous tasks (Cipriani et al., 2011a; Resnik et al., 2012, 2014). In addition to positioning the arm in space, an important challenge is to be able to control the pre-shaping of fingers during grasping. Recent advances such as targeted muscle reinnervation (TMR) (Kuiken et al., 2009) and myoelectric control using residual limb muscle activity offer exciting possibilities (Cipriani et al., 2011a, 2014; Resnik et al., 2014). Brain-machine interfaces, which directly translate neural activity in the cortex to control external devices, may increase the level of natural control currently available in myoelectric prostheses (Lebedev and Nicolelis, 2006; Contreras-Vidal et al., 2012).

There are currently multiple myoelectric controlled hand prostheses available commercially, such as the i-limb (Touch Bionics, UK), the (FDA approved) DEKA arm (Deka integrated solutions corporation, USA) and the (FDA approved) Axon-Bus Peripheral System/Michelangelo hand (Otto Bock Healthcare Product GmbH, Austria). In In this study, we used the IH2 Azurra, a hand prosthesis developed as research platform at Prensilia s.r.l., Italy. Amputee-relevant behavioral testing methods have so far focused on peripheral neural interfaces (Zhou et al., 2007). Notably, EMG-based systems have shown reasonably reliable 7- DOF control of a prosthetic limb using EMG after targeted muscle reinnervation (TMR) – a surgical technique pioneered by Dr. Kuiken involving the

transfer of residual nerves in the amputated arm to the remaining muscle, which then provide EMG signals that correlate to the original nerve functions allowing a virtual or physical prosthetic arm to respond directly and more naturally to the brain signals (Kuiken et al., 2009; Li et al., 2010). However, some critical challenges of this approach concern the stability of EMG recordings, interference from muscles controlling remaining joints, effects of tissue loading, control of fine dexterous movements, and the cognitive burden of operating the device (Kuiken et al., 2009). Other studies have shown that dexterous control of robotic hands is possible using surface/intramuscular EMG from the muscles in the residual limb (Cipriani et al., 2014).

Recent milestones in BMI research include real-time cortical control of robotic limbs in monkeys (Musallam et al., 2004; Taylor et al., 2002; Kim et al., 2006; Serruya et al., 2002), non-human primates (Carmena et al., 2003; Velliste et al., 2008; Clanton et al., 2010) and the control of 2D/3D computer cursors by able bodied and/or paralyzed individuals (Hochberg et al., 2006; McFarland et al., 2010; Bradberry et al., 2011; Schalk et al., 2008; Ganguly and Carmena, 2009) . Hochberg et al (2006) reported results for a tetraplegic human (MN) implanted with a 96-microelectrode array in the primary motor cortex (MI). Subject MN was able to achieve, in the course of 57 consecutive sessions over 9 months, BMI control of 2D cursor movement that MN used to open and close email, operate devices such as a television and open and close a prosthetic hand to grasp and transport an object from one location to another. More recently, results from two tetraplegics demonstrating their ability to control 3D reach and grasp movements with the DEKA robotic arm (Resnik et al., 2014) were published (Hochberg et al., 2012). Collinger et al., 2012 showed that over a period of 13 weeks, a tetraplegic could learn to control a robotic arm with 7 degrees of freedom (including 1 for grasping) in 3D space. Overall, intracranial BMIs have showed control of arm positioning with a high degree of accuracy in tetraplegic users, but have a single degree of freedom to control grasping

(Hochberg et al., 2012; Collinger et al., 2012; Velliste et al., 2008). In amputees who are able to produce muscular activity in residual limbs, intracortical BMIs present an unfavorable risk to benefit ratio compared to myoelectric prosthetics. In such cases, noninvasive BMIs to control prosthetic limbs could potentially augment myoelectric control, but have not been demonstrated yet.

Proximal and distal upper extremity movement information has been shown to be encoded as the power in specific frequency bands in cortical field potentials at different spatial scales: local field potentials (LFPs), electrocorticography (ECoG), electroencephalography (EEG) and magnetoencephalography (MEG) (Zhuang et al., 2010; Kubánek et al., 2009; Pistohl et al., 2012; Ball et al., 2008; Waldert et al., 2009). More recently, researchers have shown that information is also encoded in the time-domain amplitudes of these field potentials in the lowest frequency band (0-5 Hz) (Mollazadeh et al., 2011; Bansal et al., 2011; Acharya et al., 2010; Kubánek et al., 2009; Bradberry et al., 2010, 2009; Hall et al., 2014). In our previous work we show that grasping movements in able-bodied individuals can be decoded from time-domain low delta-band (0.1 – 1 Hz) electroencephalographic (EEG) activity, a noninvasive modality to record cortical potentials at the scalp (Agashe and Contreras-Vidal, 2011, 2013a; Paek et al., 2014). Further, we showed that principal components (PCs) of finger kinematics are decoded with the same level of accuracy as finger joint angles during grasp pre-shaping. In a closed-loop BMI scenario, it is advantageous to control the kinematic PCs as they allow grasp pre-shaping with fewer degrees of freedom.

In recent years, concerns over the long-term stability of intracortical neural recordings have been raised, and studies show a decrease in BMI performance over time (Chestek et al., 2011; Dickey et al., 2009; Perge et al., 2014). In intracortical implanted electrode studies, changes in recorded signals and the resulting changes in BMI performance are attributed to formation of scar tissue and migration of neurons, as

well as unstable electrode material characteristics (Chestek et al., 2011; Dickey et al., 2009). (Simeral et al., 2011) investigated the stability and reliability of intracortical microelectrode arrays in a human with tetraplegia 1000 days post- implantation and showed viable recordings for decoding and satisfactory performance of a cursor control task during five consecutive days of testing. The same subject S3 also demonstrated continuous neuronal ensemble control of simulated arm reaching using a Kalman decoder in days 1049, 1057, and 1080 post-implant (Chadwick et al., 2011). Chao et al., 2010 evaluated ECoG- based decoding of hand position and arm joint angles during reaching movements in non-human primates over a period of several months. This study showed that decoding performance did not significantly degrade with time and that decoding performance and the time between decoder model generation and decoder testing were not negatively correlated. (Perge et al., 2014) studied two tetraplegics implanted with multi-electrode arrays over the period of one year. Decoding accuracy during a motor imagery task declined at the rate of 3.6[5.65]%/month (for subjects T2 and [S3] respectively), using a multi-unit spiking activity based decoder. For LFP-based decoder, a similar decline (2.4[2.85]%/month) was reported.

In the case of EEG, the reasons for session-to-session variability are different: variability in electrode placement, gradual changes in impedance between scalp and electrodes due to changes in environmental conditions such as humidity, temperature, channel motion, and sweat, and changes in emotional, hormonal and pharmacological states of subjects. However, similar questions regarding the long-term signal quality and BMI performance hold in the case of EEG, and have not yet been investigated. In this study, we look at stability of EEG signals as well as changes in BMI performance over multiple sessions performed on different days in two chronic transradial amputees.

Figure 3.1 Experimental setup. Amputee participants were fitted with the IH2 Azurra robotic hand to their residual limb sockets. Sixty-four channel active EEG was recorded simultaneously while participants performed the grasping task.

3.2 Materials and methods

Study participants

This study was approved by the institutional review board at the University of Houston. Two amputee volunteers participated in this study after giving written informed consent. The inclusion criteria for this study were: a) Traumatic transradial amputation in right arm b) Right hand dominant before amputation c) No untreated pain/neuromas in residual limb and no untreated phantom pain e) Should be able to carry weight of prosthetic (640 g) fitted to their stump socket. Participant A1 was a 56 years old healthy male who underwent bilateral transradial upper limb amputation following an electrocution injury 32 years before this study. At the time of testing, he used a body-powered hook prosthetic which he had been using for the past 25 years. Participant A2 was a 59 years old woman who underwent right transradial upper limb amputation following an automotive accident 14 years before this study. At the time of testing, she used a myoelectric controlled electric hook prosthetic which she had been using for the past 14 years. Both participants did not show any indications of cognitive deficits, and were right hand dominant before amputation. Participant A1 was under supervised pharmacological treatment to manage hypertension and urinary bladder function. Participant A2 was under supervised pharmacological treatment for depression,

hormone imbalance, pain management (for phantom pain as well as shoulder joint inflammation) and drug dependence. Both participants did not report any changes in

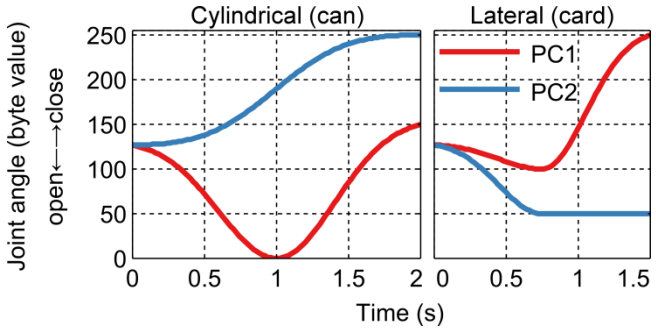

Figure 3.2 PC1 and PC2 training phase trajectories. Pre-determined trajectories during the training phase were based on two synergies of movement, PC1 and PC2. PC1 controlled the flexion/extension of the fingers and the thumb, while PC2 controlled the thumb rotation.

phantom sensation on the residual limb during the experiment.

Data acquisition

Participants were fitted with an anthropomorphic prosthetic hand (IH2 Azurra, Prensilia s.r.l., Italy) to their residual limb sockets (Figure 3.1) fitted by a CPO specialist. Whole head 64 channel active EEG (BrainAmpDC with actiCAP, Brain Vision LLC, USA) was recorded at 100 Hz during the experiment. Simultaneous recording of EEG, real-time data processing, and control of the robotic hand was achieved using the BCI2000 software framework (Schalk et al., 2004). Although EEG was recorded at 100 Hz, data packets were sent from EEG amplifiers at a rate 50 Hz, constraining the real-time loop to 20 ms. Consequently, robotic hand control was also sampled at 50 Hz.

The IH2 Azurra robotic hand has five degrees of freedom (dof): one each for the flexion-extension of the thumb, index finger and middle finger, one for the combined flexion-extension of the ring and little finger, and one for the thumb rotation (Cipriani et al., 2011b). The IH2 Azurra hand uses a differential mechanism via which a single dof is used to control both the MCP (metacarpal-phalangeal) and PIP (proximal inter-phalangeal) finger joints in such a way that when the MCP joint encounters an

obstruction (due to grasping an object), the PIP continues to flex until the object is fully grasped (Cipriani et al., 2011a). Finger kinematics for a single dof were specified at an 8-bit resolution, with 0 and 255 corresponding to open and fully flexed positions respectively. Nominally, two synergies of grasping based on principal component analysis of the joint angles were identified based on previous work (Agashe and Contreras-Vidal, 2011; Santello et al., 1998) corresponding to the correlated movement of the flexion-extension across all fingers and the thumb (PC1), and the thumb rotation (PC2).

Experiment design

Participants performed 13 sessions over a period of 5 weeks, with each session being performed on a different day. In the first 6 sessions, participants performed a 'training' phase (used to create a BMI decoder) followed by a 'testing' phase (closed loop control using the decoder created in the training phase). In the next 6 sessions (sessions 7 – 12), only the testing phase was performed, using the decoder from the training phase of the 6^{th} session. The first 6 sessions allowed us to investigate the changes in decoders over multiple days, while the sessions 7-12 allowed us to investigate the adaptability of the brain to a fixed decoder, the consistency of the EEG signals, and any changes in BMI performance across multiple sessions. The final (13^{th}) session was used to measure chance levels for the continuous time predictions: blind to participants, computer-generated Brownian noise was used to control the robotic hand, instead of participants' EEG, while they attempted to do so.

Participants were seated at a table with their attached robotic hand resting on a flat switch, which served to synchronize onset of hand transport and EEG decoder output controlling grasp preshaping. During the behavioral task, participants grasped an object (either an aluminum water bottle or a credit card, corresponding to cylindrical and lateral grasps respectively) with the robotic hand. Each trial consisted of the researcher

presenting an object to be grasped at a pre-determined comfortable distance (20-30 cm) away from the resting position. Following presentation of the object to be grasped,

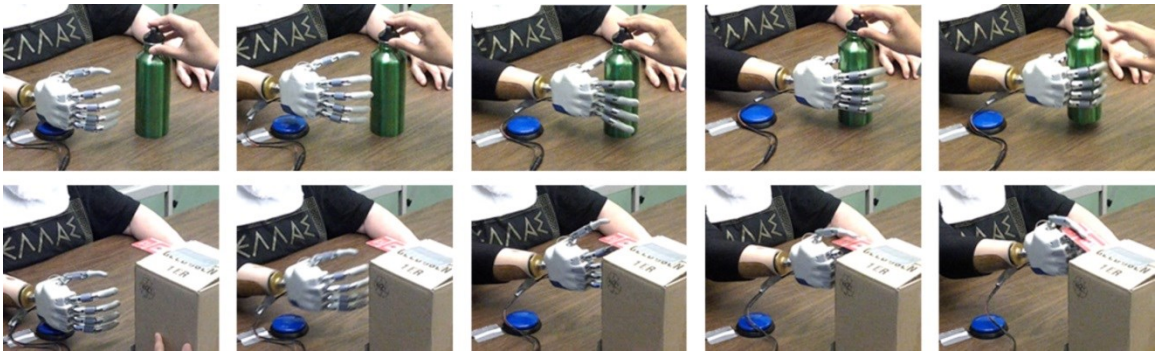

Figure 3.3 Grasp trajectories in the training phase. Snapshots of the grasp trajectory are shown above for thy cylindrical grasp (top row) and the lateral grasp (bottom row).

participants self-initiated hand transport towards the object.

During the training phase, initiation of hand transport triggered a pre-determined grasping sequence in the robotic hand, suitable to the object being presented. The pre-determined finger joint trajectories were created so as to have typical human grasp aperture time profiles seen during grasping (Castiello, 2005). A Gaussian profile was used for PC1 activation, while a Gaussian profile was used for PC2 velocity, with a total time lengths 2 s and 1.5 s respectively (Figure 3.2). The thumb rotation (PC2) was held constant during the second half of the trajectory in the case of the lateral grasp. Participants timed their hand transport in conjunction with hand pre-shaping, so that the object was grasped by the end of the hand transport. Participants were instructed to imagine themselves controlling the hand pre-shaping and grasping. In addition to the visual feedback, participants were asked to imagine kinesthetic feedback as well. The grasp was held steady for 2 s, followed by an opening of the grasp and a return to the resting position (reverse of the grasping trajectory). During the grasp release trajectory, participants transported the hand back to its resting position (Figure 3.3). Participants

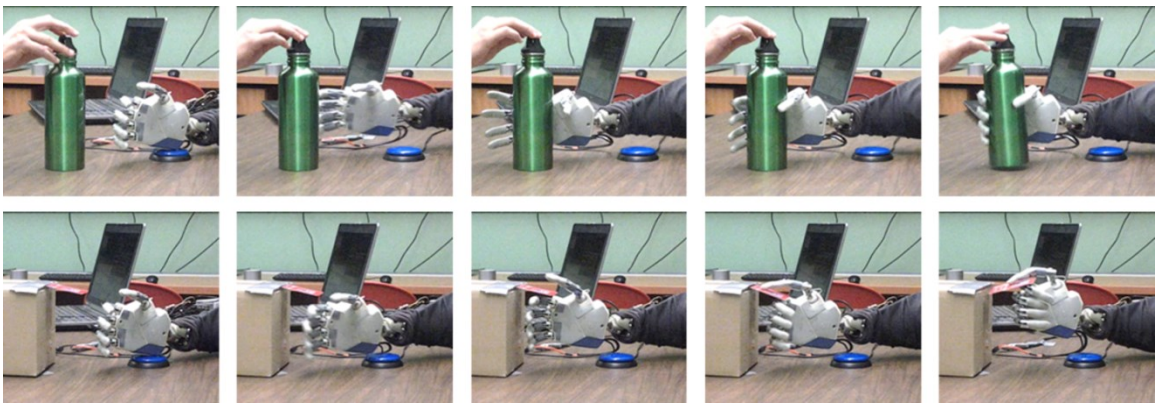

Figure 3.4 Grasp pre-shaping with closed loop control. Examples of successful grasps during the closed-loop control are shown for the cylindrical (top row) and the lateral (bottom row) grasps .

performed 100 trials during the training phase. The order in which objects (bottle or card) were presented varied in a pseudorandom fashion.

A mapping between the 64-channel EEG data and the two synergies (PC1 and PC2) was created using data recorded in the training phase. In the testing phase, this mapping was applied to EEG to make real-time predictions of PC1 and PC2, allowing closed-loop control of the robotic hand pre-shaping. Initiation of hand transport by the participant, following presentation of an object to be grasped, triggered the start of closed-loop control (Figure 3.4). Thereafter, participants had 5 s to grasp the presented object. The outcome of each trial was marked as a ‘success’ or ‘failure’ depending on whether the participant was able to grasp the object or not within the allotted preset time (5 s). Monitoring current drawn by the actuator motor for each degree of freedom allowed us to detect when an object was grasped, since the current drawn spikes up if resistance due to the object is encountered. Once an object was successfully grasped, closed loop control ceased and the grasp was held steady for 2 s. Following either outcome, the hand shape was returned to resting position according to the pre-determined grasp release trajectory suitable for the presented object, as used in the training phase.

Signal processing

A causal filter was used to band-pass filter data between 0.1 -1 Hz. This was implemented as cascaded high pass and low pass 2nd order Butterworth filters. The maximum group phase delay in the passband was 300 ms. Both training phase and testing phase EEG were filtered in this manner. After the training phase, EEG and kinematics were extracted and processed offline in MATLAB (The Mathworks Inc., USA). A lag of 100 ms was introduced in the EEG so that kinematics at time t aligned with EEG at time $t - 100$ ms. This was done to account for the cortico-spinal delay; the lag estimate was based on previous decoding studies (Bradberry et al., 2010). EEG data were standardized by their mean and standard deviation. Kinematics were upsampled to 100 Hz (from 50 Hz) using the MATLAB *pchip* (piecewise cubic hermite interpolating polynomial) method, followed by a transformation to PC1 and PC2 by multiplying with the PC coefficient matrix for the pre-determined grasp trajectories. PC1 was set to the average of the 4 finger and thumb flexion values, corresponding to PC loadings of 0.25 for each of the 4 joints. PC2 was set to the thumb rotation value. Data were segmented into movement periods, from movement onset to completion of grasp, and concatenated along trials.

Decoding

These data were then used to construct a linear mapping using robust linear regression, which mitigates the effect of outliers by weighting them less. This method was implemented in MATLAB (The Mathworks, Inc., USA) using the *robustfit* function which uses iteratively reweighted least squares with a bisquare weighting function. PC1 and PC2 were modeled independently as a linear combination of EEG sensor data:

$$PC_i[t] = \beta_{i0} + \sum_j \beta_{ij} S_j[t - 100\,ms],$$

where $PC_i[t]$ is the i^{th} PC being decoded at time t, β_{ij} are the model parameters and S_j are the processed EEG from the j^{th} electrode. In the testing phase, this linear mapping was used to predict PC1 and PC2 values from filtered and standardized EEG. Standard deviation from the training phase was used to scale EEG. These PC predictions were then scaled using a gain parameter so that when transformed back to the kinematic space of joint actuators, they represent movements which spanned the kinematic range. A few (typically 5-10) trials were conducted before the testing phase to manually tune the gain parameters according to the subjects' preference of the range of motion. A saturation filter was applied to the output to constrain final predicted kinematic actuator values to 0-255.

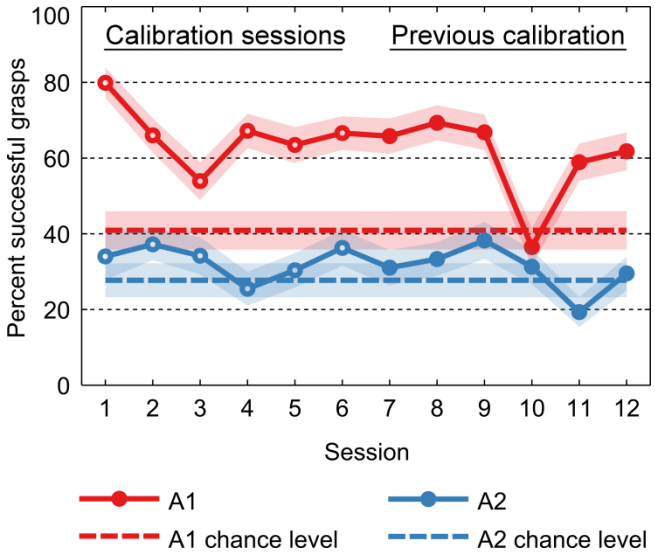

Figure 3.5 Closed loop BMI performance across sessions. The first six sessions (open circles) represent sessions in which a training phase preceded the testing phase. The last six sessions (solid circles) used the decoder calibration from the sixth session.

3.3 Results

Closed-loop grasping performance was stable over sessions

During closed loop BMI operation, participants were allowed 5 s from movement onset to grasp the presented object in each trial. If the object was grasped successfully,

we marked it as a 'success', and as a 'failure' otherwise. Figure 3.4 shows examples of successful closed-loop grasps for the two objects. We used the percentage of successful trials (success rate) within a session as a performance metric to measure BMI performance. In addition to correctly decoded kinematics, this metric also depended on the ability of participants to position and time the hand transport to successfully grasp the presented object. Correct decoding of hand grasp kinematics (finger extension followed by flexion with suitable amplitude and timing) but incorrect hand orientation resulted in a failure to grasp the object functionally, and was counted as such. Thus, while functionally relevant, success rate as a metric was a compounded measure of participants' ability to position and time the hand transport in synchrony with the decoded kinematics. The first 6 sessions included observation-based decoder training immediately preceding the closed-loop operation (see methods). In sessions 7-12, participants performed only the closed-loop control (testing) phase. In the 13th session, blind to subjects, we controlled the two synergies using Brownian noise. In this case, the success rate is an isolated measure of their ability to time their hand transport and position to successfully grasp an object, when the prosthetic hand randomly opens and closes. Brown noise was used as it spectrally similar to EEG, with the power spectra of both signals following a characteristic $\frac{1}{f^{|\alpha|}}$ curve (Nunez and Srinivasan, 2006). It should be noted that chance levels are not 50%, since the two outcomes (success vs. failure) do not necessarily have equal probabilities and because the decoding task was not discrete and depended on appropriate EEG-based scaling and timing of prosthetic grasp suitable for the test object.

Success rates were significantly above chance levels ($p < 0.05$) for participant A1, except for one session (Figure 3.5). For participant A2, success rates were significantly above chance levels in only 2 sessions. Participant A2 had greater difficulty

with hand transport, in part due to shoulder pain, resulting in lower chance levels than participant A1. Participant A2 was also under the influence of various pharmacological agents to treat her depression, pain and addition, which may have likely contributed poor signal stability and lower BMI performance. During the first 6 sessions, when the decoder was calibrated before each closed-loop phase, performance for participant A1 remained stable at 66 ± 3%, indicating that BMI performance is consistent across multiple decoders created on different days. With the exception of one session, performance for sessions 7 to 12 was also stable at 65 ± 2%, indicating that the brain is able to recall decoders from previous sessions.

Long-term stability of EEG signal features and decoders

Three factors determine BMI performance: the quality and stability of the input signals (EEG features), the decoder, and the user's changing internal states. Stability of EEG features used as inputs to the BMI across sessions has not been investigated previously. In this regard, we tracked delta-band EEG standard deviation and amplitude changes at the time scale of 10 s, across multiple sessions (Figures 3.6A, B) for participant A1 who had BMI performance above chance levels. We did not observe any discernible differences between the observation-based calibration phases and the closed-loop phase. Across all sessions, EEG amplitude is higher in the prefrontal and temporal scalp regions, likely due to high amplitude ocular and myographic artifacts. One of the sessions (session 9) had high EEG amplitudes and standard deviation across all scalp regions, but did not correspond to lower BMI performance. EEG features were also stable over time scales relevant for decoding (100 ms), and across sessions with differing BMI performance (Figure 3.6C).

To visualize the changes in the decoders across the first 6 sessions for participant A1, we plotted the model parameters on a scalp map for PC1 and PC2 (Figure 3.7). In each BMI calibration (training) phase, models were created so as to

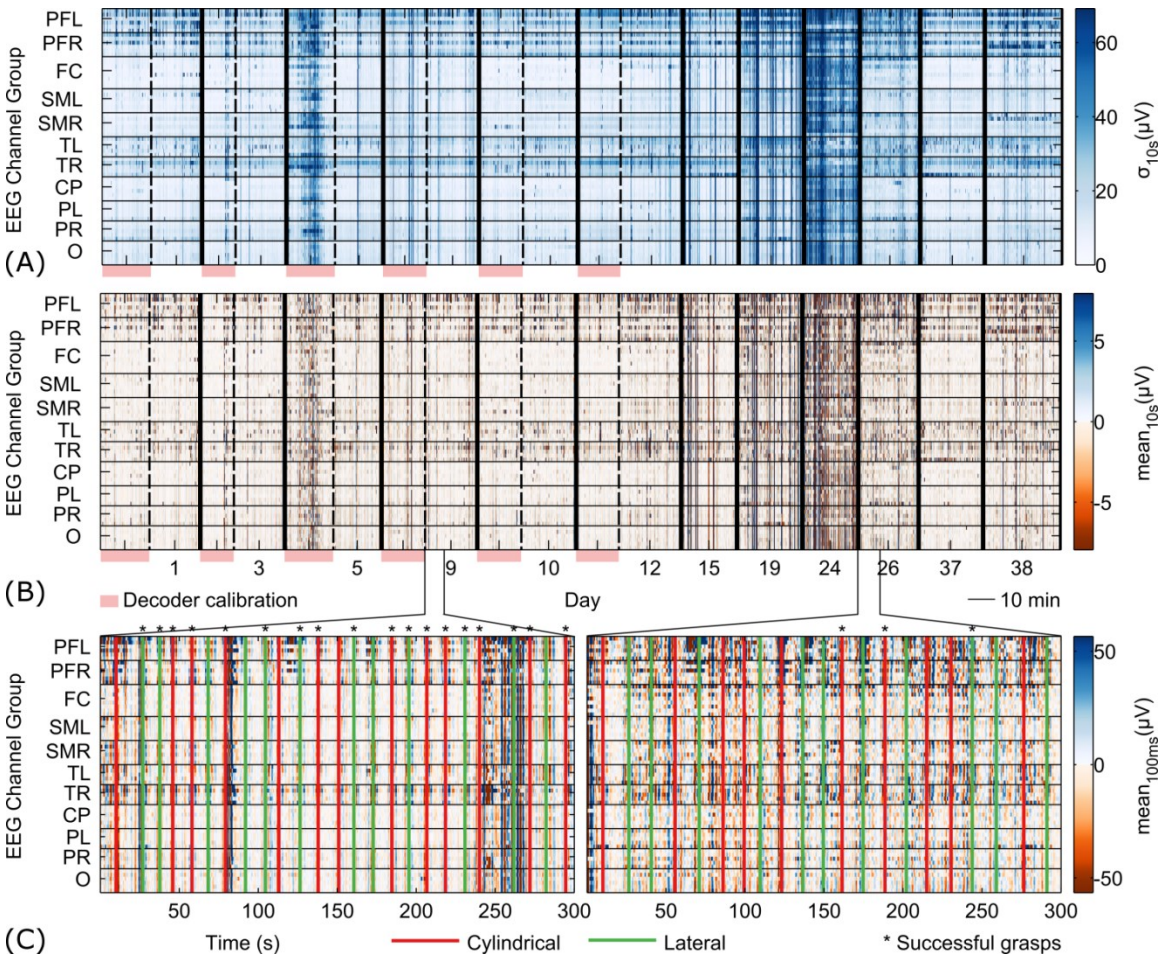

Figure 3.6 Longitudinal stability of EEG (participant A1). (A) Shows the standard deviation in the delta band, at a timescale of 10s. (B) Shows the mean at the same timescale. (C) Shows the changes in EEG at the timescale of 100 ms (timescale relevant for decoding).

minimize the least square error between the model predicted and actual kinematic trajectories. Since the BMI performance was stable, changes in the model over sessions indicates underlying EEG signal changes. Interestingly, although models for PC1 and PC2 were created independently, they showed very similar sets of EEG channels over which the magnitude of model parameters was high, within each session (Figure 3.7). This indicates that signals over similar scalp areas control both PC1 and PC2 amplitudes, and is expected from the smoothly coordinated and temporally coupled synergies during natural grasping (Santello et al., 1998, 2002).

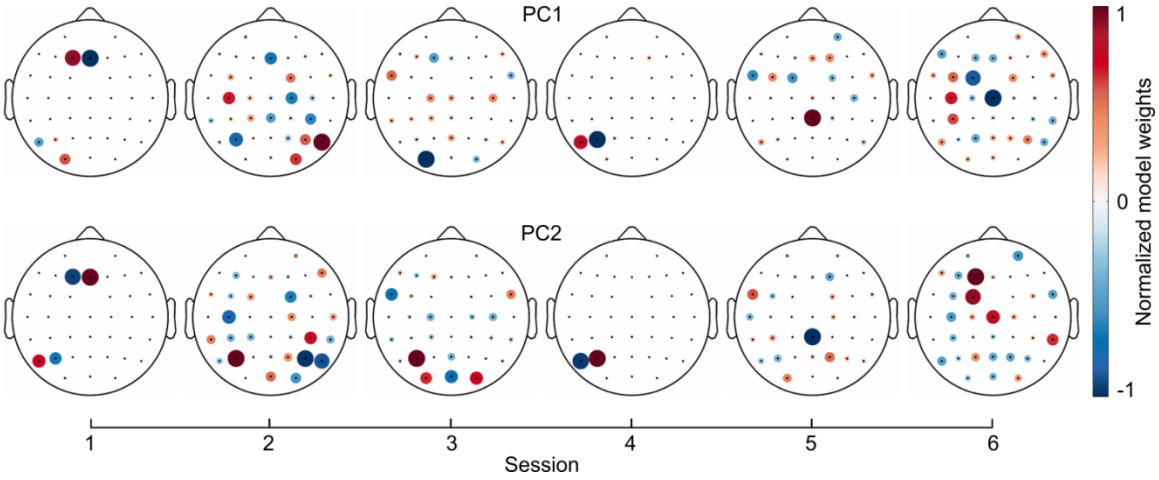

Figure 3.7 Stability of decoder across sessions (participant A1). For the first 6 sessions, BMI decoders were calibrated after the training phase. BMI decoder parameters for PC1 (top row) and PC2 (bottom row) were plotted on a scalp map.

3.4 Discussion

Closed-loop BMI performance

Over all sessions, BMI success rate was 63 ± 3% for participant A1 (above chance levels in 11 sessions) and 32 ± 2% for participant A2 (above chance levels in 2 sessions). With a fixed decoder (sessions 7-12), the success rate was 60 ± 5% for participant A1 (above chance levels in 5 sessions) and 30 ± 3% for participant A2 (above chance levels in 1 session). Participant A2 was under pharmacological treatment for depression, hormone imbalance, pain management (for phantom pain as well as shoulder joint inflammation) and drug dependence. Pharmacological interventions for depression and pain management, and hormonal interventions are known to affect global brain activity as measured in EEG (Hunter et al., 2006; Becker et al., 1980; Guisado et al., 1975), and may explain the lower BMI performance levels in participant A2. In addition, shoulder pain resulted in participant A2 being unable at times to smoothly coordinate hand transport. These conditions may represent useful exclusion criteria for future EEG-based neuroprosthetics.

In the absence of overt kinematics in amputees, being able to train decoders presents a challenge for researchers. In the past, movement observation has been used to train BMI models in primates for 3D reaching movements (Wahnoun et al., 2004, 2006). A similar approach has been used to calibrate intracortical BMI systems to control positioning of an arm in space in humans (Hochberg et al., 2012). Bradberry et al., 2011 have shown that it is possible to use action observation to determine a mapping between noninvasive EEG activity and cursor movement on a computer screen. We show in this study that observing grasping actions performed by a robotic hand can be used to train time-domain EEG-based neural interfaces, allowing amputees to grasp objects.

Closed-loop BMI and EEG stability

Learning to use a BMI is similar to learning a new tool (Bradberry et al., 2011). Given a new fixed decoder, neural patterns have been shown to change over sessions, resulting in an increase in BMI performance (up to a limit) as the brain learns the new 'tool' (Carmena et al., 2003). Over larger time scales of months, BMI performance may also decay, owing to loss in signal quality (Perge et al., 2014). A complementary approach to keeping the decoder fixed and letting the brain adapt is to adapt the decoder itself to changing neural activity, such that BMI performance is maximized (Orsborn et al., 2012). There is typically a characteristic time-scale associated with changes in BMI performance over sessions due to changes in neural patterns, and a time-scale at which the BMI model is adaptive (Digiovanna et al., 2009). In our study, we used two extremes on the closed-loop BMI system adaptation time-scale spectrum: the first 6 sessions, when the decoder was changed every session, represents the fastest time-scale (single session), while sessions 7-12, when a fixed decoder was used, represent the other extreme in which adaptation was limited to the user's brain.

Changing the decoder every session is generally accepted to be detrimental to BMI performance (Orsborn et al., 2012), and strategies have been proposed to make

optimal use of the interaction between the adaptive BMI algorithm and the learning process of the brain itself (Digiovanna et al., 2009; Orsborn et al., 2012). Nevertheless, we created a new decoder every session for the first six sessions as we wanted to study the stability of such decoder over sessions, with respect to the input EEG features. Our results show that as a result of changing EEG features, decoders are not stable. The performance drop in session 3 for participant A1 could possibly be associated with unstable EEG signal quality during the training phase for this session (Figure 3.6A, B) During sessions 7-12, the decoder was fixed, allowing us to examine the potential for cortical plasticity, given that performance was stable, except for one session. Surprisingly, the performance was stable for this duration, and possibly because the time-scale of BMI user learning may be longer than 6 sessions (Hochberg et al., 2012; Collinger et al., 2012; Perge et al., 2014).

Implications for noninvasive BMIs

In this study, an amputee participant (A1) was able to control a robotic hand to grasp two objects (bottle and credit card) with a success rate of 63% over 5 weeks. We previously showed that low-frequency time domain EEG contains information about a variety of upper limb movement intentions, such as hand transport (Bradberry et al., 2010), grasping (Agashe and Contreras-Vidal, 2011, 2013a), and finger movements (Paek et al., 2014). Studies from other groups show similar results from field potentials at smaller spatial scales, like LFPs (Zhuang et al., 2010; Mollazadeh et al., 2011; Bansal et al., 2011; Hall et al., 2014) and ECoG (Acharya et al., 2010; Kubánek et al., 2009; Pistohl et al., 2012). Closed-loop studies with implanted intracortical electrodes also show significant information in low-frequency time-domain LFP (Perge et al., 2014). Here, we show for the first time that this feature space is viable for extracting grasping-related movement intent from amputees, and can be used to control closed-loop neuroprosthetics.

Our current BMI relies on subject-initiated hand transport to trigger BMI control of the hand via a switch, constraining the system to laboratory use. BMI systems able to detect initiation of hand transport for grasping without a switch, would be more suited for use outside the lab is a target for future innovation. Further studies with a larger time window that will be able to detect changes in BMI learning over the scale of months are also needed. Tactile feedback from fingertip sensors may also help neuroprosthetic embodiment and closed-loop performance. Further studies are also needed to investigate the generalizability of decoders to different grasp types. Results from this study show that EEG-based BMIs are feasible when the right input feature space is used.

CHAPTER 4: CONCLUSION

Current myoelectric control of upper limb prosthetics allows reasonable control over arm positioning and orientation. Brain machine interfaces which directly translate cortical activity to control prosthetic devices may augment existing myoelectric control by allowing natural and intuitive control. Current BMI technology is invasive and requires the use of implanted microelectrodes to access cortical signals and is restricted to tetraplegics. Here we develop a noninvasive (EEG-based) BMI for prosthetic control and demonstrate its feasibility in amputees.

Representation of grasping kinematics at the macro scale of EEG has not been investigated previously. Here, we show that low frequency (0.1 – 1 Hz) time domain EEG encodes grasping kinematics accurately. Specifically, we were able to show high correlation between predicted and actual trajectories of finger joint angle velocity synergies during grasp pre-shaping. In addition to synergies, we also demonstrated high accuracies for individual joint angular velocities. The spatio-temporal pattern of recruitment of scalp areas was found to be in agreement with previously known neurophysiological correlates of motor control. Information content in EEG about the grasp type peaked at 250 ms after movement onset. The high decoding accuracies in this study are significant not only as evidence for time-domain modulation in macro-scale brain activity, but for the field of brain-machine interfaces as well. Our decoding strategy, which harnesses the neural 'symphony' as opposed to local members of the neural ensemble (as in intracranial approaches), may provide a means of extracting information about motor intent for grasping without the need for penetrating electrodes.

Using the low frequency time domain EEG feature space, we designed a closed-loop BMI with which an amputee participant (A1) was able to control a robotic hand to grasp two objects (bottle and credit card) with a success rate of 63%. Here, we show for the first time that this feature space is viable for extracting grasping-related movement

intent from amputees, and can be used to control closed-loop neuroprosthetics. Further investigation is required to ascertain stability of BMI models and EEG over longer time scales. Further studies are also needed to investigate the generalizability of BMI models to different grasp types. Results from this study show that EEG-based BMIs are feasible when the right input feature space is used.

REFERENCES

Acharya, S., Fifer, M. S., Benz, H. L., Crone, N. E., and Thakor, N. V (2010). "Electrocorticographic Amplitude Predicts Finger Positions During Slow Grasping Motions of the Hand." *J. Neural Eng*. 7, 046002. doi:10.1088/1741-2560/7/4/046002.

Agashe, H. A., and Contreras-Vidal, J. L. (2013a). "Decoding the Evolving Grasping Gesture from Electroencephalographic (EEG) Activity." *Eng. Med. Biol. Soc. (EMBC), 2013 35th Annu. Int. Conf. IEEE 2013*, 5590–3. doi:10.1109/EMBC.2013.6610817.

Agashe, H. A., and Contreras-Vidal, J. L. (2013b). "Observation-based Calibration of Brain-Machine Interfaces for Grasping." *6th Int. IEEE EMBS Conf. Neural Eng*., 1–4. doi:10.1109/NER.2013.6695856.

Agashe, H. A., and Contreras-Vidal, J. L. (2011). "Reconstructing Hand Kinematics During Reach to Grasp Movements from Electroencephalographic Signals." *Eng. Med. Biol. Soc. (EMBC), 2011 33th Annu. Int. Conf. IEEE 2011*, 5444–7. doi:10.1109/IEMBS.2011.6091389.

Aggarwal, V., Acharya, S., Tenore, F., Shin, H.-C., Etienne-Cummings, R., Schieber, M. H., and Thakor, N. V (2008). "Asynchronous Decoding of Dexterous Finger Movements Using M1 Neurons." *IEEE Trans. Neural Syst. Rehabil*. Eng. 16, 3–14. doi:10.1109/TNSRE.2007.916289.

Antelis, J. M., Montesano, L., Ramos-Murguialday, A., Birbaumer, N., and Minguez, J. (2013). "On the Usage of Linear Regression Models to Reconstruct Limb Kinematics from Low Frequency EEG Signals." *PLoS One* 8, 61976. doi:10.1371/journal.pone.0061976.

Artemiadis, P. K., Shakhnarovich, G., Vargas-Irwin, C. E., Donoghue, J. P., and Black, M. J. (2007). "Decoding Grasp Aperture from Motor-Cortical Population Activity." *Conference Proceedings: IEEE/EMBS Conference on Neural Engineering*, 518–521.

Ball, T., Demandt, E., Mutschler, I., Neitzel, E., Mehring, C., Vogt, K., Aertsen, A., and Schulze-Bonhage, A. (2008). "Movement Related Activity in the High Gamma Range of the Human EEG." *Neuroimage* 41, 302–10. doi:10.1016/j.neuroimage.2008.02.032.

Bansal, A. K., Vargas-Irwin, C. E., Truccolo, W., and Donoghue, J. P. (2011). "Relationships Among Low-Frequency Local Field Potentials, Spiking Activity, and Three-Dimensional Reach and Grasp Kinematics in Primary Motor and Ventral Premotor Cortices." *J. Neurophysiol*. 105, 1603–19. doi:10.1152/jn.00532.2010.

Becker, D., Creutzfeldt, O. D., Schwibbe, M., and Wuttke, W. (1980). "Electrophysiological and Psychological Changes Induced by Steroid Hormones in Men and Women." *Acta Psychiatr. Belg*.

Birbaumer, N. (2006). "Breaking the Silence: Brain–Computer Interfaces (BCI) for Communication and Motor Control." *Psychophysiology* 43, 517–532.

Bradberry, T. J., Contreras-Vidal, J. L., and Rong, F. (2008). "Decoding Hand and Cursor Kinematics from Magnetoencephalographic Signals During Tool Use." *Conf. Proc. IEEE Eng. Med. Biol. Soc. 2008*, 5306–9. doi:10.1109/IEMBS.2008.4650412.

Bradberry, T. J., Gentili, R. J., and Contreras-Vidal, J. L. (2011). "Fast Attainment of Computer Cursor Control with Noninvasively Acquired Brain Signals." *J. Neural Eng*. 8, 036010. doi:10.1088/1741-2560/8/3/036010.

Bradberry, T. J., Gentili, R. J., and Contreras-Vidal, J. L. (2010). "Reconstructing Three-Dimensional Hand Movements from Noninvasive Electroencephalographic Signals." *J. Neurosci*. 30, 3432–7. doi:10.1523/JNEUROSCI.6107-09.2010.

Bradberry, T. J., Rong, F., and Contreras-Vidal, J. L. (2009). "Decoding Center-Out Hand Velocity from MEG Signals During Visuomotor Adaptation." *Neuroimage* 47, 1691–700. doi:10.1016/j.neuroimage.2009.06.023.

Carmena, J. M., Lebedev, M. A., Crist, R. E., O'Doherty, J. E., Santucci, D. M., Dimitrov, D. F., Patil, P. G., Henriquez, C. S., and Nicolelis, M. A. L. (2003). "Learning to Control a Brain-Machine Interface for Reaching and Grasping by Primates." *PLoS Biol*. 1, E42. doi:10.1371/journal.pbio.0000042.

Castiello, U. (2005). "The Neuroscience of Grasping." *Nat. Rev. Neurosci*. 6, 726–36. doi:10.1038/nrn1744.

Chadwick, E. K., Blana, D., Simeral, J. D., Lambrecht, J., Kim, S. P., Cornwell, a S., Taylor, D. M., Hochberg, L. R., Donoghue, J. P., and Kirsch, R. F. (2011). "Continuous Neuronal Ensemble Control of Simulated Arm Reaching by a Human with Tetraplegia." *J. Neural Eng*. 8, 034003. doi:10.1088/1741-2560/8/3/034003.

Chao, Z. C., Nagasaka, Y., and Fujii, N. (2010). "Long-Term Asynchronous Decoding of Arm Motion Using Electrocorticographic Signals in Monkeys." *Front. Neuroeng*. 3, 3. doi:10.3389/fneng.2010.00003.

Chestek, C. a, Gilja, V., Nuyujukian, P., Foster, J. D., Fan, J. M., Kaufman, M. T., Churchland, M. M., Rivera-Alvidrez, Z., Cunningham, J. P., Ryu, S. I., et al. (2011). "Long-Term Stability of Neural Prosthetic Control Signals from Silicon Cortical Arrays in Rhesus Macaque Motor Cortex." *J. Neural Eng*. 8, 045005. doi:10.1088/1741-2560/8/4/045005.

Cipriani, C., Antfolk, C., Controzzi, M., Lundborg, G., Rosén, B., Carrozza, M. C., and Sebelius, F. (2011a). "Online Myoelectric Control of a Dexterous Hand Prosthesis by Transradial Amputees." *Neural Syst. Rehabil. Eng. IEEE Trans*. 19, 260–270.

Cipriani, C., Controzzi, M., and Carrozza, M. C. (2011b). "The SmartHand Transradial Prosthesis." *J. Neuroeng. Rehabil*. 8, 29. doi:10.1186/1743-0003-8-29.

Cipriani, C., Segil, J., Birdwell, J., and Weir, R. (2014). "Dexterous Control of a Prosthetic Hand Using Fine-Wire Intramuscular Electrodes in Targeted Extrinsic Muscles." *IEEE Trans. neural Syst. Rehabil. Eng*. 22.4: 826-836. doi: 10.1109/TNSRE.2014.2301234

Clanton, S. T., Zohny, Z., Velliste, M., and Schwartz, A. B. (2010). "Simultaneous 7-Dimensional Cortical Control of an Arm and Hand Robot Via Direct Brain Interface." *Neuroscience Meeting Planner. San Diego, CA: Society for Neuroscience*, 2010, Program No. 494.6.

Collinger, J. L., Wodlinger, B., Downey, J. E., Wang, W., Tyler-Kabara, E. C., Weber, D. J., McMorland, A. J., Velliste, M., Boninger, M. L., and Schwartz, A. B. (2012). "High-Performance Neuroprosthetic Control by an Individual with Tetraplegia." *Lancet* 6736, 1–8. doi:10.1016/S0140-6736(12)61816-9.

Contreras-Vidal, J. L., Presacco, A., Agashe, H. A., and Paek, A. (2012). "Restoration of Whole Body Movement: Toward a Noninvasive Brain-Machine Interface System." *IEEE Pulse* 3, 34.

Delorme, A., and Makeig, S. (2004). "EEGLAB: An Open Source Toolbox for Analysis of Single-Trial EEG Dynamics Including Independent Component Analysis." *J. Neurosci. Methods* 134, 9–21. doi:10.1016/j.jneumeth.2003.10.009.

Dickey, A. S., Suminski, A., Amit, Y., and Hatsopoulos, N. G. (2009). "Single-Unit Stability Using Chronically Implanted Multielectrode Arrays." *J. Neurophysiol*. 102, 1331–9. doi:10.1152/jn.90920.2008.

Digiovanna, J., Member, S., Mahmoudi, B., Fortes, J., Principe, J. C., and Sanchez, J. C. (2009). "Coadaptive Brain – Machine Interface via reinforcement learning." *Biomedical Engineering, IEEE Transactions on* 56.1 (2009): 54-64.

Ganguly, K., and Carmena, J. M. (2009). "Emergence of a Stable Cortical Map for Neuroprosthetic Control." *PLoS Biol*. 7, e1000153. doi:10.1371/journal.pbio.1000153.

Garipelli, G., Chavarriaga, R., and Millán, J. D. R. (2013). "Single Trial Analysis of Slow Cortical Potentials: A Study on Anticipation Related Potentials." *J. Neural Eng*. 10, 036014. doi:10.1088/1741-2560/10/3/036014.

Goncharova, I., McFarland, D., Vaughan, T., and Wolpaw, J. (2003). "EMG Contamination of EEG: Spectral and Topographical Characteristics." *Clin. Neurophysiol*. 114, 1580–1593. doi:10.1016/S1388-2457(03)00093-2.

Gönen, M., and Alpaydın, E. (2011). "Multiple Kernel Learning Algorithms." *J. Mach. Learn. Res*. 12, 2211–2268.

Guisado, R., Arieff, A. I., Massry, S. G., Lazarowitz, V., and Kerian, A. (1975). "Changes in the Electroencephalogram in Acute Uremia. Effects of Parathyroid Hormone and Brain Electrolytes." *J. Clin. Invest*. 55, 738.

Hall, T. M., de Carvalho, F., and Jackson, A. (2014). "A Common Structure Underlies Low-Frequency Cortical Dynamics in Movement, Sleep, and Sedation." *Neuron*, 1–15. doi:10.1016/j.neuron.2014.07.022.

Hamed, B. S., Schieber, M. H., and Pouget, A. (2007). "Decoding M1 Neurons During Multiple Finger Movements." *J. Neurophysiol*. 98, 327–33. doi:10.1152/jn.00760.2006.

Hochberg, L. R., Bacher, D., Jarosiewicz, B., Masse, N. Y., Simeral, J. D., Vogel, J., Haddadin, S., Liu, J., Cash, S. S., and van der Smagt, P. (2012). "Reach and Grasp by People with Tetraplegia Using a Neurally Controlled Robotic Arm." *Nature* 485, 372–375.

Hochberg, L. R., Serruya, M. D., Friehs, G. M., Mukand, J. A., Saleh, M., Caplan, A. H., Branner, A., Chen, D., Penn, R. D., and Donoghue, J. P. (2006). "Neuronal

Ensemble Control of Prosthetic Devices by a Human with Tetraplegia.” *Nature* 442, 164–171. doi:10.1038/nature04970.

Hunter, A., Leuchter, A., Morgan, M., and Cook, I. (2006). "Changes in Brain Function (Quantitative EEG Cordance) During Placebo Lead-in and Treatment Outcomes in Clinical Trials for Major Depression.” *Am. J. Psychiatry* 163, 1426–1432.

Jeannerod, M. (1984). "The Timing of Natural Prehension Movements.” *J. Mot. Behav*. 16, 235–254.

Kim, S. P., Sanchez, J. C., Rao, Y. N., Erdogmus, D., Carmena, J. M., Lebedev, M. A., Nicolelis, M. A. L., and Principe, J. C. (2006). "A Comparison of Optimal MIMO Linear and Nonlinear Models for Brain-Machine Interfaces.” *J. Neural Eng*. 3, 145–161.

Kubánek, J., Miller, K. J., Ojemann, J. G., Wolpaw, J. R., and Schalk, G. (2009). "Decoding Flexion of Individual Fingers Using Electrocorticographic Signals in Humans.” *J. Neural Eng*. 6, 066001. doi:10.1088/1741-2560/6/6/066001.

Kuiken, T. A., Li, G., Lock, B. A., Lipschutz, R. D., Miller, L. A., Stubblefield, K. A., and Englehart, K. B. (2009). "Targeted Muscle Reinnervation for Real-Time Myoelectric Control of Multifunction Artificial Arms.” *JAMA J. Am. Med. Assoc*. 301, 619–628.

Lebedev, M. A., and Nicolelis, M. A. L. (2006). "Brain-Machine Interfaces: Past, Present and Future.” *Trends Neurosci*. 29, 536–546. doi:10.1016/j.tins.2006.07.004.

Li, G., Schultz, A. E., and Kuiken, T. A. (2010). "Quantifying Pattern Recognition-Based Myoelectric Control of Multifunctional Transradial Prostheses.” *Neural Syst. Rehabil. Eng. IEEE Trans*. 18, 185–192.

Linderman, M., Lebedev, M. A, and Erlichman, J. S. (2009). "Recognition of Handwriting from Electromyography.” *PLoS One* 4, e6791. doi:10.1371/journal.pone.0006791.

Matsumura, M., Kawashima, R., Naito, E., Satoh, K., Takahashi, T., Yanagisawa, T., and Fukuda, H. (1996). "Changes in rCBF During Grasping in Humans Examined by PET." *Neuroreport* 7, 749–752.

McFarland, D. J., Sarnacki, W. A., and Wolpaw, J. R. (2010). "Electroencephalographic (EEG) Control of Three-Dimensional Movement." *J. Neural Eng*. 7, 36007.

Mollazadeh, M., Aggarwal, V., Davidson, A. G., Law, A. J., Thakor, N. V, and Schieber, M. H. (2011). "Spatiotemporal Variation of Multiple Neurophysiological Signals in the Primary Motor Cortex During Dexterous Reach-to-Grasp Movements." *J. Neurosci*. 31, 15531–43. doi:10.1523/JNEUROSCI.2999-11.2011.

Murata, A., Fadiga, L., Fogassi, L., Gallese, V., Raos, V., and Rizzolatti, G. (1997). "Object Representation in the Ventral Premotor Cortex (Area F5) of the Monkey." *J. Neurophysiol*. 78, 2226–2230.

Musallam, S., Corneil, B. D., Greger, B., Scherberger, H., and Andersen, R. A. (2004). "Cognitive Control Signals for Neural Prosthetics." *Science* (80-.). 305, 258–262.

Nunez, P. L., and Srinivasan, R. (2006). Electric Fields of the Brain: the Neurophysics of EEG. Oxford University Press, USA.

Orsborn, A. L., Dangi, S., Moorman, H. G., Carmena, J. M., and Member, S. (2012). "Closed-Loop Decoder Adaptation on Intermediate Time-Scales Facilitates Rapid BMI Performance Improvements Independent of Decoder Initialization Conditions." *Neural Sys. and Rehab. Eng., IEEE Trans.* 20.4 (2012): 468-477 20, 468–477.

Paek, A. Y., Agashe, H. A., and Contreras-Vidal, J. L. (2014). "Decoding Repetitive Finger Movements with Brain Activity Acquired Via Non-invasive Electroencephalography." *Front. Neuroeng*. 7, 3.

Perge, J. a, Zhang, S., Malik, W. Q., Homer, M. L., Cash, S., Friehs, G., Eskandar, E. N., Donoghue, J. P., and Hochberg, L. R. (2014). "Reliability of Directional Information

in Unsorted Spikes and Local Field Potentials Recorded in Human Motor Cortex.” *J. Neural Eng*. 11, 046007. doi:10.1088/1741-2560/11/4/046007.

Pistohl, T., Schulze-Bonhage, A., Aertsen, A., Mehring, C., and Ball, T. (2012). "Decoding Natural Grasp Types from Human ECoG.” *Neuroimage* 59, 248–60. doi:10.1016/j.neuroimage.2011.06.084.

Quian Quiroga, R., and Panzeri, S. (2009). "Extracting Information from Neuronal Populations: Information Theory and Decoding Approaches.” *Nat. Rev. Neurosci*. 10, 173–85. doi:10.1038/nrn2578.

Rakotomamonjy, A., Bach, F., Canu, S., and Grandvalet, Y. (2008). "SimpleMKL.” *J. Mach. Learn. Res*. 9, 2491–2521.

Resnik, L., Borgia, M., Latlief, G., Sasson, N., and Smurr-Walters, L. (2014). "Self-Reported and Performance-Based Outcomes Using DEKA Arm.” *J. Rehabil. Res. Dev*. 51, 351–362.

Resnik, L., Meucci, M. R., Lieberman-Klinger, S., Fantini, C., Kelty, D. L., Disla, R., and Sasson, N. (2012). "Advanced Upper Limb Prosthetic Devices: Implications for Upper Limb Prosthetic Rehabilitation.” *Arch. Phys. Med. Rehabil*. 93, 710–717.

Rizzolatti, G., Camarda, R., Fogassi, L., Gentilucci, M., Luppino, G., and Matelli, M. (1988). "Functional Organization of Inferior Area 6 in the Macaque Monkey.” *Exp. brain Res*. 71, 491–507.

Rizzolatti, G., Fadiga, L., Matelli, M., Bettinardi, V., Paulesu, E., Perani, D., and Fazio, F. (1996). "Localization of Grasp Representations in Humans by PET: 1. Observation Versus Execution.” *Exp. brain Res*. 111, 246–252.

Saleh, M., Takahashi, K., Amit, Y., and Hatsopoulos, N. G. (2010). "Encoding of Coordinated Grasp Trajectories in Primary Motor Cortex.” *J. Neurosci*. 30, 17079–17090.

Santello, M., Flanders, M., and Soechting, J. F. (2002). "Patterns of Hand Motion During Grasping and the Influence of Sensory Guidance." *J. Neurosci*. 22, 1426–1435.

Santello, M., Flanders, M., and Soechting, J. F. (1998). " Postural Hand Synergies for Tool Use." *J. Neurosci*. 18, 10105.

Schalk, G., McFarland, D. J., Hinterberger, T., Birbaumer, N., and Wolpaw, J. R. (2004). "BCI2000: A General-Purpose Brain-Computer Interface (BCI) System." *Biomed. Eng. IEEE Trans*. 51, 1034–1043. doi:10.1109/TBME.2004.827072.

Schalk, G., Miller, K. J., Anderson, N. R., Wilson, J. a, Smyth, M. D., Ojemann, J. G., Moran, D. W., Wolpaw, J. R., and Leuthardt, E. C. (2008). "Two-Dimensional Movement Control Using Electrocorticographic Signals in Humans." *J. Neural Eng*. 5, 75–84. doi:10.1088/1741-2560/5/1/008.

Schultz, A. E., and Kuiken, T. A. (2011). "Neural Interfaces for Control of Upper Limb Prostheses: The State of the Art and Future Possibilities." *PM&R* 3, 55–67.

Serruya, M. D., Hatsopoulos, N. G., Paninski, L., Fellows, M. R., and Donoghue, J. P. (2002). "Brain-Machine Interface: Instant Neural Control of a Movement Signal." *Nature* 416, 141–142.

Shawe-Taylor, N., and Kandola, A. (2002). "On Kernel Target Alignment." *Adv. Neural Inf. Process. Syst*. 14, 367.

Simeral, J. D., Kim, S.-P., Black, M. J., Donoghue, J. P., and Hochberg, L. R. (2011). "Neural Control of Cursor Trajectory and Click by a Human with Tetraplegia 1000 Days After Implant of an Intracortical Microelectrode Array." *J. Neural Eng*. 8, 025027. doi:10.1088/1741-2560/8/2/025027.

Snoek, G. J., IJzerman, M. J., Hermens, H. J., Maxwell, D., and Biering-Sorensen, F. (2004). "Survey of the Needs of Patients with Spinal Cord Injury: Impact and Priority for Improvement in Hand Function in Tetraplegics." *Spinal Cord* 42, 526–32. doi:10.1038/sj.sc.3101638.

Taylor, D. M., Tillery, S. I. H., and Schwartz, A. B. (2002). "Direct Cortical Control of 3D Neuroprosthetic Devices." *Science* (80-.). 296, 1829.

Theiler, J., Eubank, S., Longtin, A., Galdrikian, B., and Doyne Farmer, J. (1992). "Testing for Nonlinearity in Time Series: The Method of Surrogate Data." *Phys. D Nonlinear Phenom.* 58, 77–94.

Townsend, B. R., Subasi, E., and Scherberger, H. (2011). "Grasp Movement Decoding from Premotor and Parietal Cortex." *J. Neurosci*. 31, 14386–98. doi:10.1523/JNEUROSCI.2451-11.2011.

Vargas-Irwin, C. E., Shakhnarovich, G., Yadollahpour, P., Mislow, J. M. K., Black, M. J., and Donoghue, J. P. (2010). "Decoding Complete Reach and Grasp Actions from Local Primary Motor Cortex Populations." *J. Neurosci*. 30, 9659–9669. doi:10.1523/JNEUROSCI.5443-09.2010.

Velliste, M., Perel, S., Spalding, M. C., Whitford, A. S., and Schwartz, A. B. (2008). "Cortical Control of a Prosthetic Arm for Self-Feeding." *Nature* 453, 1098–101. doi:10.1038/nature06996.

Vinjamuri, R., Sun, M., Chang, C.-C., Lee, H.-N., Sclabassi, R. J., and Mao, Z.-H. (2010). "Dimensionality Reduction in Control and Coordination of the Human Hand." *IEEE Trans. Biomed. Eng*. 57, 284–295.

Wahnoun, R., He, J., and Helms Tillery, S. I. (2006). "Selection and Parameterization of Cortical Neurons for Neuroprosthetic Control." *J. Neural Eng*. 3, 162–71. doi:10.1088/1741-2560/3/2/010.

Wahnoun, R., Tillery, S. I. H., and He, J. (2004). "Neuron Selection and Visual Training for Population Vector Based Cortical Control." *Eng. Med. Biol. Soc. 2004. IEMBS '04. 26th Annu. Int. Conf. IEEE* 2, 4607–4610. doi:10.1109/IEMBS.2004.1404277.

Waldert, S., Pistohl, T., Braun, C., Ball, T., Aertsen, A., and Mehring, C. (2009). "A Review on Directional Information in Neural Signals for Brain-Machine Interfaces." *J. Physiol. Paris* 103, 244–54. doi:10.1016/j.jphysparis.2009.08.007.

Wolpaw, J. R., and McFarland, D. J. (2004). "Control of a Two-Dimensional Movement Signal by a Noninvasive Brain-Computer Interface in Humans." *PNAS* 101, 17849.

Yuan, H., Perdoni, C., and He, B. (2010). "Relationship Between Speed and EEG Activity During Imagined and Executed Hand Movements." *J. Neural Eng*. 7, 26001. doi:10.1088/1741-2560/7/2/026001.

Zhou, P., Lowery, M. M., Englehart, K. B., Huang, H., Li, G., Hargrove, L., Dewald, J. P. a, and Kuiken, T. a (2007). "Decoding a New Neural Machine Interface for Control of Artificial Limbs." *J. Neurophysiol*. 98, 2974–82. doi:10.1152/jn.00178.2007.

Zhuang, J., Truccolo, W., Vargas-Irwin, C. E., and Donoghue, J. P. (2010). "Decoding 3-D Reach and Grasp Kinematics from High-Frequency Local Field Potentials in Primate Primary Motor Cortex." *IEEE Trans. Biomed. Eng*. 57, 1774–84. doi:10.1109/TBME.2010.2047015.